JOURNAL OF GEOPHYSICAL RESEARCH, VOL. 112, F03005, doi:10.1029/2006JF000617, 2007

Two-diffusion description of hyperpycnal deltas

Steven Y. J. Lai[1] and Hervé Capart[1]

Received 27 June 2006; revised 16 November 2006; accepted 10 January 2007; published 19 July 2007.

[1] Alluvial deltas formed upstream of lakes and reservoirs often exhibit concave foresets with maximum inclinations smaller than the angle of repose. In the present work, we test whether this morphology could be attributed to bed load sediment transport by turbid underflows, acting along the foreset beds before their fine sediment load settles out of suspension. Under hyperpycnal conditions, both the topset and foreset of the delta would thus be subject to the geomorphic influence of the dense river inflow. To describe this joint geomorphic action by subaerial and subaqueous currents, we derive a two-diffusion theory and modify it to account for inclination thresholds. Different diffusion strengths apply to the topset and foreset, on either side of the moving shoreline. For a channel of uniform initial slope and a constant water level in the body of standing water, we show that the resulting moving boundary problem admits exact similarity solutions. To test the theory, the analytical solutions are compared with small-scale laboratory experiments in which turbid underflows are replaced by brine currents. The curved profiles predicted by the theory and measured in the experiments resemble those of surveyed deltaic deposits in lakes known to be prone to turbidity currents.

Citation: Lai, S. Y. J., and H. Capart (2007), Two-diffusion description of hyperpycnal deltas, *J. Geophys. Res.*, *112*, F03005, doi:10.1029/2006JF000617.

1. Introduction

[2] As alluvial rivers enter bodies of standing water, loss of sediment transport capacity typically leads to the formation of delta-shaped deposits. When the water level varies little or stays constant, these delta deposits gradually prograde into the body of standing water. Upstream, subaerial streamflow proceeds along the aggrading topset bed and supplies sediment to the advancing shoreline. Downstream of this shoreline, the nature of the subaqueous deposits is influenced by the density of the river inflow relative to the receiving ambient. For homopycnal and hypopycnal flows, in which the entering discharge is either neutrally buoyant or lighter than the ambient, a sudden reduction in tractive force along the bed is experienced at the shoreline. This leads to steep-sloped foreset deposits controlled by angle-of-repose avalanching of coarser bed sediment, leaving the finer suspended fractions to settle out further downstream as bottomset beds. Such deltas, and their topset-foreset-bottomset architecture, were first described in a classical work by *Gilbert* [1890], and are accordingly known as Gilbert-type deltas.

[3] Hyperpycnal flows, on the other hand, occur when the inflowing discharge is denser than the receiving ambient. This commonly occurs when floodwaters laden with fine sediment enter freshwater lakes. In that case, the denser inflow will plunge down the lake bottom and continue its path in the form of a density current. Because stable density stratification inhibits turbulent entrainment [*Ellison and Turner*, 1959], such density currents tend to keep their identity rather than thoroughly mix with the overlying ambient. This allows turbidity currents to travel over considerable distances, decaying primarily because of a gradual settling out of their fines content [*Bell*, 1942]. They may also reach the deep end of the lake, ponding into underwater turbid pools which then slowly detrain their clear water and sediment their solid particles.

[4] As they plunge along the lake bed, hyperpycnal flows can exert a significant geomorphic influence on the delta front, inducing for instance the formation of bed forms [*Bornhold and Prior*, 1990]. Among other features, the foresets of hyperpycnal deltas tend to have much milder inclinations than their Gilbert-type counterparts [*Kostic et al.*, 2002]. Such geomorphic influence suggests that turbidity currents have the ability to drive along-bed motions of coarser grains, much like subaerial streams have the power to transport bed load [*Syvitski et al.*, 2007]. Laboratory experiments by A. Cantelli and B. Yu (see the video in chapter 4 of the electronic book by *Parker* [2004]) confirm that such transport can indeed occur at the base of turbid underflows.

[5] As a natural example, consider the case of the Alpine Rhine River (Alpenrhein) at Lake Constance (Bodensee). During flood conditions, the Rhine carries into the lake a large suspended load composed of 10% clay, 70% silt, and 20% sand, at concentrations of up to 6000 mg/l [*Müller and Förstner*, 1966; *Roth et al.*, 2001]. This inflow generates turbidity currents along the bottom, with underflow velocities of more than 1 m/s [*Lambert*, 1982], carrying the clay and silt fractions to the deeper parts of the lake [*Roth et al.*, 2001]. The associated deltaic morphology is illustrated in

[1]Department of Civil Engineering and Hydrotech Research Institute, National Taiwan University, Taipei, Taiwan.

0148-0227/07/2006JF000617$09.00

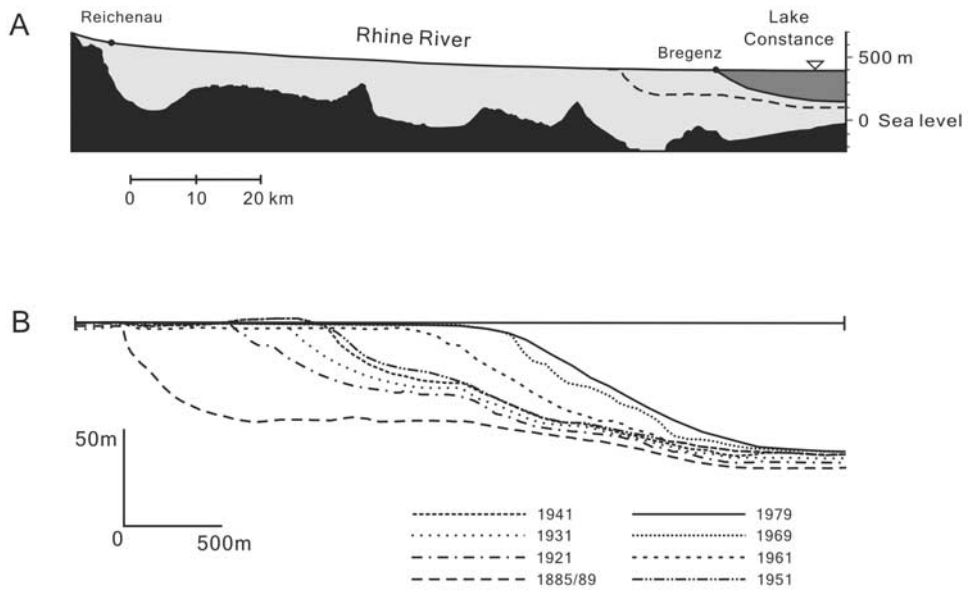

Figure 1. Rhine River delta at Lake Constance, Switzerland: (a) present subaerial and subaqueous long profile of the Rhine [after *Hinderer*, 2001] and (b) progradation of the subaqueous delta foreset from 1885/89 to 1979 [after *Kenyon and Turcotte*, 1985] (data from work by *Müller* [1966], supplemented by more recent profiles from the work of *Hinderer* [2001]).

Figure 1a. Upstream of the shoreline, the long profile of the Rhine River plain exhibits a mild inclination and a slightly concave curvature. At the shoreline, a sharp break of slope is observed. Downstream, the subaqueous foreset exhibits a steeper gradient and a concave profile of more marked curvature. Near the shoreline break, the maximum inclination of the foreset is of the order of 6° [*Adams et al.*, 2001], much greater than the topset slope but well below typical angles of repose. Toward the deep end of the lake, the leading edge of the foreset bed connects smoothly with the lake bathymetry. The shape of the delta front thus differs significantly from Gilbert's description. Plotted in Figure 1b, the recorded evolution of the delta front between 1885/89 and 1979 further shows that foresets have maintained a similar morphology over almost a century of progradation.

[6] In an influential paper, *Kenyon and Turcotte* [1985] recognized that this kind of foreset morphology and its time evolution could be described mathematically as the product of a diffusion process. Kenyon and Turcotte, however, identified bulk transport (creep or landslides) as the geomorphic agent responsible for the subaqueous diffusion. Although they included the case of Lake Constance in their field examples, they did not consider the possibility that turbidity currents could be responsible instead. In the present paper, our objective is to examine this alternative mechanism. Specifically, we aim to test whether the geomorphic action of dense underflows could account for the observed long profile of the Rhine Delta, and for the morphology of other deltas in lakes known to be prone to turbidity currents. Other field examples where density currents appear to control the subaqueous delta morphology include the Colorado River delta in Lake Mead [*Grover and Howard*, 1937; *Smith et al.*, 1960] and the Noeick River delta in a fjord of the British Columbia Coast [*Bornhold and Prior*, 1990]. More recent discussions of the Lake Mead case can be found in work by *Graf* [1971] and *Kostic and Parker* [2003a].

[7] Despite their importance documented in a variety of field studies [*Wright et al.*, 1988; *Fan and Morris*, 1992], hyperpycnal deltas have been the focus of few theoretical and experimental studies. Numerical models have been proposed by Syvitski and coworkers [e.g., *Syvitski and Alcott*, 1993; *Syvitski and Hutton*, 2001; *Kubo et al.*, 2005] and by *Kostic and Parker* [2003a]. Laboratory experiments known to us are limited to the studies by *Yu et al.* [2000], *Kostic et al.* [2002], *Kostic and Parker* [2003b], and *Toniolo and Schultz* [2005], with the latter three references documenting data from the same experimental setup. This contrasts with the more diverse studies devoted to Gilbert-type deltas. In recent years alone, mathematical and numerical models have been proposed by *Swenson et al.* [2000], *Parker and Muto* [2003], *Voller et al.* [2004], *Bellal et al.* [2005], and *Capart et al.* [2007]. Laboratory experiments with steep foreset deltas controlled by angle-of-repose avalanching have also been presented recently by *Muto* [2001], *Bellal et al.* [2003], *Muto and Swenson* [2005], *Kleinhans* [2005], and *Kim et al.* [2006]. One aim of the present work is to extend to hyperpycnal deltas some of the mathematical and experimental techniques applied to Gilbert-type deltas in these recent studies.

[8] As discussed above, turbidity currents carry fine sediments which gradually settle out of suspension, and simultaneously they can drive a basal transport of coarser grains. This dual role played by the currents complicates both theoretical developments and experimental interpretations. For this reason, our approach in the present paper will be to ignore the first process, and focus only on the second. We will assume that the fines fraction of the turbidity

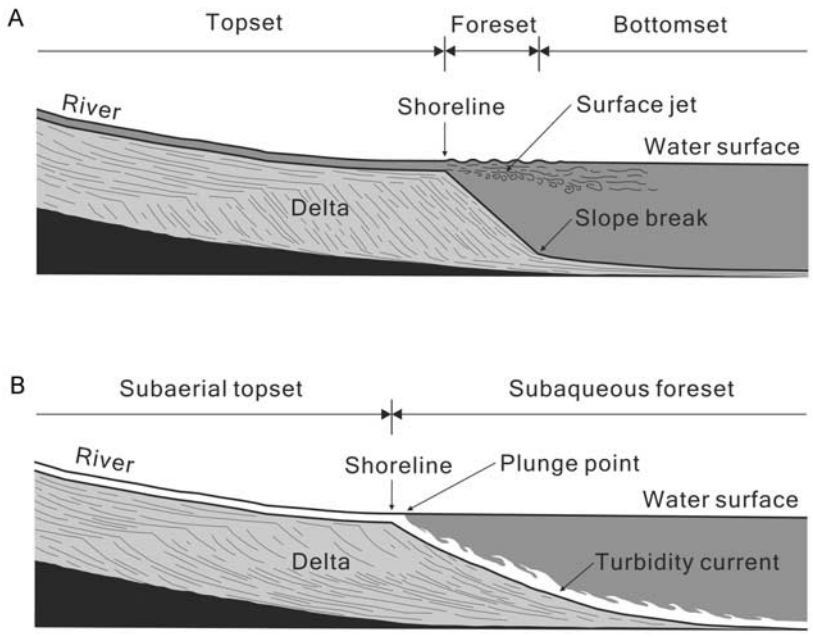

Figure 2. Alluvial deltas under homopycnal and hyperpycnal conditions: (a) classical Gilbert-type delta obtained under homopycnal inflow [after *Gilbert*, 1890] and (b) hyperpycnal delta evolving under the joint geomorphic action of steady river flow (along the topset) and a sustained turbidity underflow (along the foreset).

current (responsible for the density contrast with the ambient water) settles out of suspension at a very slow rate. As a result, we will not consider the long-range delivery or long-term settling of these fines, nor consider the resulting formation of bottomset beds. Instead, we will focus exclusively on the upstream geomorphic influence exerted by the turbid underflows on the coarser-grained foresets. This simplified picture is illustrated in Figure 2b, where it is contrasted with the Gilbert-type delta described earlier (Figure 2a).

[9] Our simplified view of hyperpycnal deltas (Figure 2b) is motivated by the fact that the two processes, sedimentation of fine particles and basal transport of coarser grains, develop over different timescales in certain field cases. In the Shihmen reservoir of Taiwan, for example, flood discharges carrying fine sediment exert a geomorphic influence on the upstream deltaic deposit only over the days immediately following intense typhoon rainfall [*Lee et al.*, 2006], whereas weeks are required for the settling of the turbid pool accumulated at the deep end of the reservoir [*Hsu*, 2006]. Accordingly, for the laboratory experiments presented in this paper, we will replace the turbid currents by brine currents, and focus exclusively on the geomorphic consequences of basal sand transport by the dense currents.

[10] The paper is structured as follows. In section 2, we start from elementary assumptions regarding the hyperpycnal flow and sediment bed response to derive a diffusion approximation of the delta morphodynamics. The result of the derivation is a two-diffusion description of the delta evolution, with distinct diffusion strengths along the topset and foreset. On the basis of heuristic arguments, an identical mathematical formulation was earlier proposed by *Jordan and Flemings* [1991] to describe the long-term evolution (over geological timescales) of foreland basins. *Marr et al.* [2000] also recently applied a two-diffusion model to gravel-sand transitions in depositional basins. In order to better approximate the experimental results, we modify the two-diffusion formulation slightly to take into account the effect of inclination thresholds.

[11] In section 3, we show that, under certain restrictions on the initial and boundary conditions, the mathematical equations can be solved exactly. To achieve this, we exploit symmetries of the diffusion equation that were earlier used by *Voller et al.* [2004] and *Capart et al.* [2007] to obtain analytical solutions for Gilbert-type deltas. Section 4 is devoted to a presentation of the laboratory experiments conducted to test the theory. For this purpose, we compare the measured long profiles of small-scale hyperpycnal deltas with the analytical solutions. Photographs are also presented to illustrate the delta behavior when the ratio of inflow density to lake density changes. In section 5, finally, we summarize the paper and propose some conclusions.

2. Theory

[12] With reference to Figure 2b, we adopt the following simplifying assumptions to describe hyperpycnal deltas. First, a valley of constant width is assumed, allowing us to focus exclusively on the one-dimensional development of the long profile. Sustained inflows of turbid water and bed load sediments are considered upstream of the delta, and the ambient water in the lake is assumed homogenous. The delta morphology is taken to evolve sufficiently slowly that both the subaerial and subaqueous currents adjust in a quasi-

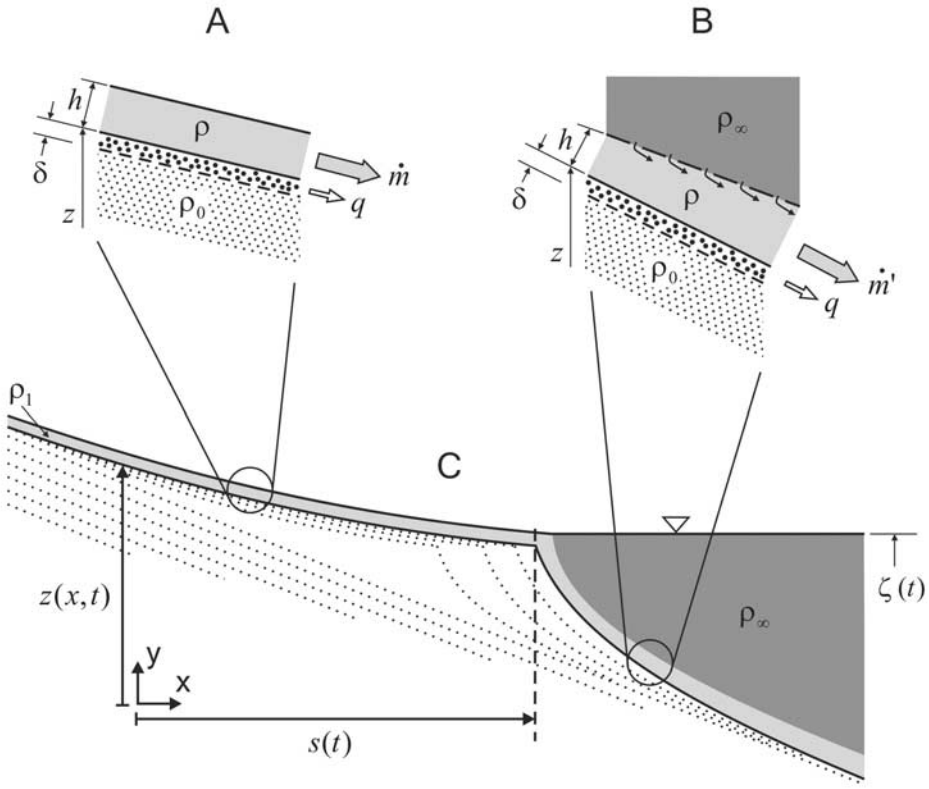

Figure 3. Definition sketch: (a) normal flow along the topset, (b) normal flow along the foreset, and (c) coevolving topset and foreset.

steady manner. The bed curvature is considered sufficiently mild that the flow approaches normal conditions governed only by the local inclination and overall throughflow.

[13] We assume that the flow depths are small compared to the height of the delta front, and shallow with respect to the topset and foreset lengths. This is motivated by conditions encountered in the field, where turbidity underflows can often be considered shallow compared to the length traveled by the currents along the foreset. Two examples from British Columbia are the Noeick River delta [*Bornhold and Prior*, 1990], where underflow depths of about 10 to 20 m (reconstructed on the basis of antidune wavelengths) can be compared with a subaqueous delta length of 4 km, and the Lillooet River delta in Lillooet Lake [*Best et al.*, 2005], where sediment-laden underflows having a thickness of 13.5 m (on the basis of direct velocity profile measurements) were observed to travel down the curved delta front for distances of at least 400 m.

[14] As discussed in the introduction, one further assumption key to the present work is that the fine sediments which endow the inflow with its excess density settle out very slowly. This allows us to neglect the fallout and resulting deposition of bottomset beds (assumed to occur deeper into the reservoir outside the domain of interest). A number of other complications are excluded from the start, such as the details of the hyperpycnal flow near the plunge point [*Lee and Yu*, 1997], the effects of 3D bathymetry on the routing of the turbidity currents [*De Cesare et al.*, 2001], and the possible density stratification of the lake ambient [*Young et al.*, 2005].

[15] Figure 3 provides a definition sketch for the different variables used in the derivation. The key variable of interest is the evolving bed profile $z(x, t)$, governed by the one-dimensional Exner equation

$$\frac{\partial z}{\partial t} + \frac{\partial q}{\partial x} = 0. \tag{1}$$

This equation expresses mass conservation of the bed sediment material, assumed to have constant porosity. Variable $q(x, t)$ is the volume flux of bed load per unit width. For simplicity, the porosity and density of the bed load layer are assumed to be the same as those of the underlying sediment deposit.

[16] Normal flow is assumed along the subaerial topset. The bottom shear stress τ thus balances the downslope component of the weight of the flowing layer according to

$$\tau = (\rho h + \rho_0 \delta) g \sin \beta, \tag{2}$$

where ρ is the density of the turbid river inflow, h is the depth of the flowing turbid layer, ρ_0 is the density of the bed

(sediment and pore water taken together), δ is the thickness of the bed load layer, g is the gravitational acceleration, and β is the local bed inclination. The bed density ρ_0 is given by

$$\rho_0 = n_0\rho + (1 - n_0)\rho' \tag{3}$$

and depends on the bed porosity n_0, the turbid fluid density ρ, and the sand density ρ'.

[17] The normal-to-bed component of the submerged weight of the bed load, on the other hand, is supported by the effective stress

$$\sigma' = (\rho_0 - \rho)\delta g \cos\beta. \tag{4}$$

Following *Fraccarollo and Capart* [2002], the Coulomb-Terzaghi yield criterion is assumed to hold at the base of the bed load sublayer, i.e.,

$$\tau = \tan\varphi\sigma', \tag{5}$$

where φ is an angle of friction set equal to the angle of repose. The thickness δ of the bed load layer relative to the total flow depth $h + \delta$ is therefore given by

$$\frac{\delta}{h+\delta} = \frac{\rho\tan\beta}{(\rho_0 - \rho)(\tan\varphi - \tan\beta)}. \tag{6}$$

If $\tan\beta \ll \tan\varphi$, that is, if the bed inclination is much milder than the angle of repose, then it follows that $\delta \ll h$, thus one can further approximate

$$\delta \approx \frac{\rho h\tan\beta}{(\rho_0 - \rho)\tan\varphi}. \tag{7}$$

This simplification will be adopted throughout the later developments. Turning to the velocities, we assume that the mean velocity v of the bed load layer is proportional to the mean velocity u of the turbid water flow

$$v = \alpha_1 u, \tag{8}$$

where $\alpha_1 < 1$ is a nondimensional parameter having a constant value to be determined from experiments or from a more detailed theory. Combining the above relations, the volumetric bed load transport rate is given by

$$q = \delta v = \frac{\alpha_1\rho h u\tan\beta}{(1 - n_0)(\rho' - \rho)\tan\varphi}. \tag{9}$$

If the discharge and density of the turbid inflow upstream of the delta are steady, if the rate at which fine particles settle out of the turbid suspension is negligibly small, and if the bed evolves sufficiently slowly for the flow to be quasi-steady, then along the topset

$$d\rho/dx = 0, \text{ and } d\dot{m}/dx = 0, \tag{10}$$

where $\dot{m} = \rho h u$ is the mass flow rate (per unit width) of the subaerial turbid flow. It follows that the values of ρ and $\dot{m}$ along the topset are purely controlled by their upstream boundary values, i.e.,

$$\rho(x) = \rho_{\text{upstream}} = \rho_1 \text{ and } \dot{m}(x) = \dot{m}_{\text{upstream}} = \rho_1 Q, \tag{11}$$

where Q denotes the volumetric discharge of turbid water (per unit width) supplied upstream of the delta. Using the geometrical identity $\tan\beta = -\partial z/\partial x$, the volumetric bed load flux (9) can be rewritten in the simple form

$$q = -D_1\frac{\partial z}{\partial x}, \tag{12}$$

where

$$D_1 = \frac{\alpha_1\rho_1 Q}{(1 - n_0)(\rho' - \rho_1)\tan\varphi} \tag{13}$$

and coefficient D_1 is a constant parameter proportional to the turbid water discharge Q. Substitution of (12) into the bed material continuity equation (1) then yields the familiar linear diffusion equation

$$\frac{\partial z}{\partial t} - D_1\frac{\partial^2 z}{\partial x^2} = 0. \tag{14}$$

This diffusional description of alluvial river morphodynamics was proposed by *Culling* [1960] and *Begin et al.* [1981]. Other derivations are possible [see *Paola*, 2000], and the one proposed above is only meant to set the stage for a similar treatment of the foreset evolution.

[18] Along the subaqueous foreset, the situation is slightly more complicated because of the submersion in a water ambient (having a constant density ρ_∞) and the possible entrainment of ambient water by the turbidity current. As a result, the flowing layer can thicken and quasi-steady flow along a slope of constant inclination will no longer be uniform, i.e., $dh/d\xi \neq 0$. In fact, experiments [*Ellison and Turner*, 1959] show that, for a quiescent ambient,

$$\frac{d}{d\xi}(hu) = Eu\,, \tag{15}$$

where ξ is the curvilinear distance measured along the bed, u is the mean velocity of the turbid underflow, and E is a nondimensional entrainment coefficient.

[19] Even when the depth varies because of entrainment, however, steady density plumes are observed to quickly adjust to a normal state similar to the normal flow of subaerial channels [*Turner*, 1973]. In this normal state, the bottom shear stress approximately balances the downslope component of the submerged weight of the density current. Along the subaqueous foreset, one can therefore write a normal flow relation similar to the subaerial relation (2), i.e.,

$$\tau \approx (\rho - \rho_\infty)gh\sin\beta\,, \tag{16}$$

where the apparent weight of the density current is reduced because of the ambient buoyancy, and where we have assumed from the start that $\delta \ll h$. Following *Turner* [1973], it can also be observed that, although the thickness, density, and velocity of the current can evolve because of

entrainment, the corresponding excess density flux (or buoyancy flux per unit width) remains constant, i.e.,

$$\frac{d(\dot{m}')}{d\xi} = 0, \tag{17}$$

where $\dot{m}' = (\rho - \rho_\infty)hu$. Let us again assume that the Coulomb-Terzaghi relation (5) holds, and that the velocity of the bed load layer is proportional to the current velocity:

$$\tau = \tan\varphi\sigma' \tag{18}$$

$$v = \alpha_2 u\,. \tag{19}$$

Here the nondimensional parameter α_2 plays the same role as parameter α_1 introduced earlier for the subaerial case. Since the velocity structure of subaqueous turbidity currents differs from the velocity structure of subaerial stream flows, we expect that the subaerial and subaqueous coefficients will not take exactly the same values, i.e., $\alpha_1 \neq \alpha_2$. Proceeding along the same lines as before, we obtain for the subaqueous bed load transport rate the revised relation

$$q = \delta v = \frac{\alpha_2(\rho - \rho_\infty)hu\tan\beta}{(1-n_0)(\rho' - \rho)\tan\varphi}\,, \tag{20}$$

and the subaqueous bed load flux can be written in the form

$$q = -D_2\frac{\partial z}{\partial x}\,, \tag{21}$$

where

$$D_2 = \frac{\alpha_2\dot{m}'}{(1-n_0)(\rho' - \rho)\tan\varphi}\,. \tag{22}$$

Along the foreset, entrainment of fresh water will cause the density of the turbid current to decrease, starting from its value $\rho = \rho_1$ at the shoreline, toward the density ρ_∞ of the ambient. This will not affect the invariant excess density flux $\dot{m}'$, but will influence somewhat the density difference $\rho' - \rho$ in the denominator of (22). If the turbidity inflow is not too dense, however, we can nevertheless approximate

$$\rho' - \rho \approx \rho' - \rho_1\,. \tag{23}$$

Consider for example the conditions of our laboratory experiments (section 4) in which $\rho_1 = 1.2$ g/ml, $\rho' = 2.7$ g/cm^3, and $\rho_\infty = 1.0$ g/ml. Even for this relatively dense brine inflow, the density difference $\rho' - \rho$ between the bed load sediment and the carrier fluid changes only from $\rho' - \rho_1 = 1.5$ g/cm^3 to $\rho' - \rho_\infty = 1.7$ g/cm^3, or less than 15%, when making the maximal assumption that the inflow at density $\rho = \rho_1$ mixes completely with the ambient $\rho \rightarrow \rho_\infty$ along the foreset.

[20] Because the excess density is entirely supplied by the turbid river inflow, we must also have at the shoreline the continuity relation

$$\dot{m}' = (\rho_1 - \rho_\infty)Q, \tag{24}$$

where Q is the turbid water discharge supplied to the delta topset. Under these assumptions, the diffusion coefficient D_2 along the foreset is given by

$$D_2 = \frac{\alpha_2(\rho_1 - \rho_\infty)Q}{(1-n_0)(\rho' - \rho_1)\tan\varphi}, \tag{25}$$

which is again constant and proportional to the turbid water discharge Q supplied to the alluvial channel upstream of the delta. Substitution into the Exner equation (1) then yields another linear diffusion equation

$$\frac{\partial z}{\partial t} - D_2\frac{\partial^2 z}{\partial x^2} = 0, \tag{26}$$

where only the value of the diffusion coefficient has changed.

[21] The mathematical form of equation (26) governing the evolution of the foreset is the same as the one adopted by *Kenyon and Turcotte* [1985] to describe bulk transport due to creep or subaqueous slides. Here, however, the proposed mechanism driving the subaqueous diffusion is bed load transport at the base of the dense underflows. The manner in which we treat the geomorphic action of turbidity currents is also different from the approach of *Kostic et al.* [2002]. Whereas these authors envision a reduction of the angle of incipient avalanching due to overriding turbidity currents, here dense underflows drive basal sediment transport, with a bed load flux that depends on the bed inclination. Consequently, whereas *Kostic and Parker* [2003a] consider avalanching foresets of reduced but constant inclination, our diffusional view allows curved foresets to develop.

[22] Comparing relations (13) and (25), the ratio of subaqueous to subaerial diffusivities is given by

$$\frac{D_2}{D_1} = \frac{\rho_1 - \rho_\infty}{\rho_1}\frac{\alpha_2}{\alpha_1}. \tag{27}$$

Provided that α_1 and α_2 are not too different from each other, it is the density ratio $(\rho_1 - \rho_\infty)/\rho_1$ which will dominate. This ratio is always smaller than 1, and much smaller than 1 for the case of dilute turbidity currents. The subaqueous diffusion coefficient is thus expected to be smaller or much smaller than its subaerial counterpart. This reflects a reduction in transport capacity when the flow goes from subaerial streamflow to subaqueous underflow, leading to the deltaic deposition. For homopycnal flow ($\rho_1 = \rho_\infty$), relation (25) yields $D_2 = 0$, and the foreset can steepen until the angle of repose is reached and avalanching takes over. In the present work, the diffusive action of the dense underflow will be assumed strong enough to keep foreset inclinations safely below this threshold.

[23] Bringing together results for the topset and foreset, the bed load flux can be written

$$q(x,t) = \begin{cases} -D_1 \partial z/\partial x, \ z(x,t) \geq \zeta(t), \\ \\ -D_2 \partial z/\partial x, \ z(x,t) \leq \zeta(t), \end{cases} \tag{28}$$

where $\zeta(t)$ denotes the lake level elevation, which in general can be a function of time. The position $s(t)$ of the shoreline is obtained as the position x where the function $z(x, t) - \zeta(t)$ is equal to zero. The combination of the Exner equation (1) with the transport relations (28) yields a two-diffusion mathematical formulation that is identical to the description proposed earlier by *Jordan and Flemings* [1991] for the modeling of foreland basins. In contrast with the above derivation, Jordan and Flemings reasoned by analogy, starting from the descriptions of *Begin et al.* [1981] and *Kenyon and Turcotte* [1985], and did not attempt to identify specific mechanisms leading to the diffusive behavior. Here we show that for hyperpycnal flows, the equations can be derived on the basis of physical assumptions about the subaerial and subaqueous currents.

[24] Qualitatively, the above equations generate profiles which are relatively close in character to the profiles of actual hyperpycnal deltas, like the Rhine Delta at Lake Constance discussed in the introduction. Quantitative comparisons with the small-scale experiments discussed in section 4, however, are rather poor. In our exploratory work, we found that substantial improvements of the fit could be obtained at relatively little cost, by slightly modifying relations (28) to include the effect of inclination thresholds. In agreement with a simplified formulation of threshold effects proposed by *Mitchell* [2006], the modified relations read

$$q(x,t) = \begin{cases} \max\left\{D_1\left(-\partial z/\partial x - S_{\min,1}\right), 0\right\}, \ z(x,t) \geq \zeta(t), \\ \\ \max\left\{D_2\left(-\partial z/\partial x - S_{\min,2}\right), 0\right\}, \ z(x,t) \leq \zeta(t), \end{cases} \tag{29}$$

where $S_{\min,1}$ and $S_{\min,2}$ are inclination thresholds below which no bed load transport takes place, applicable respectively to the topset and foreset. Alternatively, each product $-D_\alpha S_{\min,\alpha}$ can be seen as the constant term in a truncated two-term Taylor series relating the bed load discharge to the bed inclination $S = -\partial z/\partial x$. We will find in section 4 that a single slope threshold $S_{\min} = S_{\min,1} = S_{\min,2}$ provides a good approximation of our experimental results. Since this may not be the case in other experiments or in field conditions, we do not make this choice right away and provisionally allow the inclination threshold to take distinct values along the delta topset and foreset. An implication of equation (29) is that, at the shoreline,

$$q(s(t),t) = D_1\left(-\partial z/\partial x - S_{\min,1}\right) = D_2\left(-\partial z/\partial x - S_{\min,2}\right), \tag{30}$$

expressing continuity of the bed load flux at the shoreline break.

3. Analytical Similarity Solutions

[25] Although the diffusion equation applied to each half domain (topset or foreset) is linear, the moving shoreline subject to compatibility conditions (30) makes the overall delta evolution problem nonlinear. For this reason, linear superposition cannot be used to construct general solutions of the mathematical problem. Special solutions, however, can be derived by exploiting certain symmetries of the diffusion equation. In fact, under certain restrictions on the boundary and initial conditions, exact solutions exist which have the remarkable property of preserving their shapes as they evolve in time.

[26] Such self-similar solutions arise in the three geometries defined in Figure 4. The first case (Figure 4a) involves a delta prograding into a lake of constant water level, starting from a bed of uniform slope extending infinitely far upstream and downstream. The second case (Figure 4b) concerns a delta prograding into a lake of constant water level and uniform bottom slope, with a steady influx of sediment prescribed at the origin. Self-similar solutions for Gilbert-type deltas in these two geometries were earlier derived by *Voller et al.* [2004], for case B, and by *Capart et al.* [2007] for case A. In the third case (Figure 4c), finally, a delta progrades into a lake of constant depth, with a constant channel bed elevation imposed at the origin. As observed by *Swenson et al.* [2000], the evolution of Gilbert-type deltas in this geometry is highly analogous to Stefan-type melting front problems, for which a classical similarity solution due to Neumann is available [see *Carslaw and Jaeger*, 1959, p. 288; *Crank*, 1984, pp.101–103]. In all three geometries, self-similar solutions can likewise be derived for hyperpycnal deltas, and we now address in turn the cases A, B, and C.

[27] For case A, the mathematical problem to be solved is given by the following set of governing equations, initial data, and boundary conditions. Let $z_1(x, t)$ and $z_2(x, t)$ denote the bed profile elevation of the topset and foreset, respectively. Along the subaerial topset,

$$\frac{\partial z_1}{\partial t} - D_1 \frac{\partial^2 z_1}{\partial x^2} = 0, \quad -\infty < x < s(t). \tag{31}$$

Along the subaqueous foreset, on the other hand,

$$\frac{\partial z_2}{\partial t} - D_2 \frac{\partial^2 z_2}{\partial x^2} = 0, \quad s(t) < x < \infty. \tag{32}$$

Initially, the bed is assumed to have the constant inclination profile

$$z = -Sx, \ -\infty < x < \infty, \ t = 0. \tag{33}$$

Boundary conditions far upstream and far downstream of the delta are

$$\frac{\partial z_1}{\partial x} = -S, \ x \to -\infty \tag{34}$$

and

$$\frac{\partial z_2}{\partial x} = -S, \quad x \to \infty. \tag{35}$$

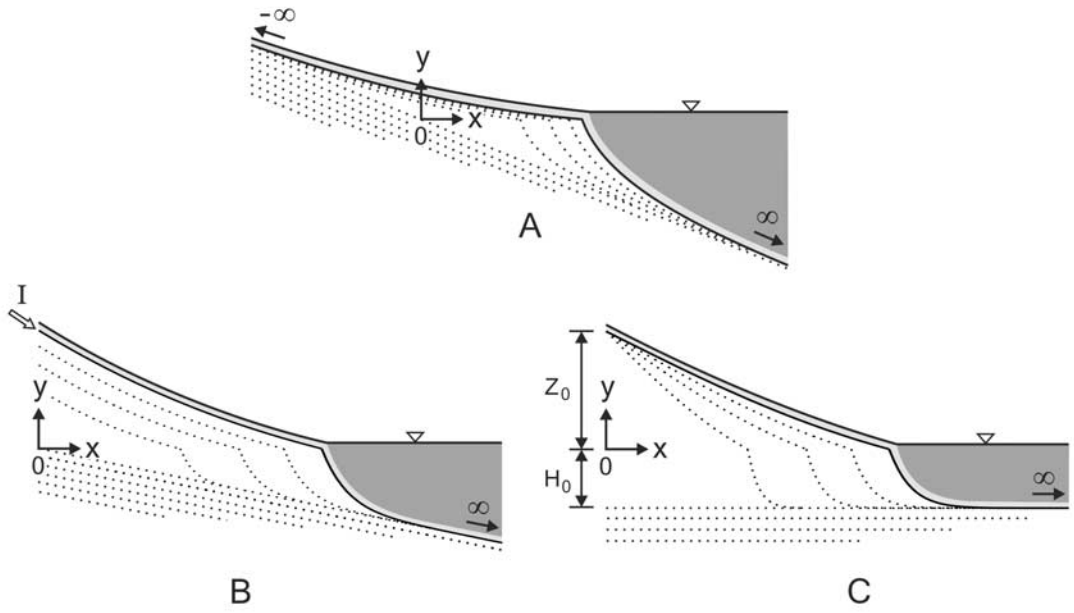

Figure 4. Three special geometries for which similarity solutions can be derived: (a) delta starting from a bed of constant slope extending infinitely far upstream and downstream; (b) delta prograding into a lake of constant bottom inclination and infinite extent, with a constant influx of sediment at the origin; and (c) delta prograding into a lake of constant depth H_0 and infinite extent, with a constant channel bed elevation Z_0 imposed at the origin.

Finally, at the shoreline, continuity of the bed profile and bed load flux requires

$$z_1 = z_2 = 0, \quad x = s(t) \tag{36}$$

$$q_1 = q_2, \quad x = s(t). \tag{37}$$

There are two ways in which the problem could be made slightly more general, yet continue to admit similarity solutions. The first would be to allow the initial bed profile to have different slopes upstream and downstream of the initial lake shoreline at $x = 0$. The second would be to let the water level in the lake evolve according to the special time history $\zeta(t) \propto \sqrt{t}$. For Gilbert-type deltas, this special type of lake level evolution was considered by *Muto and Swenson* [2005] and *Capart et al.* [2007]. For simplicity, these refinements are not considered in the present mathematical derivation.

[28] To solve the above problem, we need to jointly determine the topset and foreset profile evolutions $z_1(x, t)$ and $z_2(x, t)$. Furthermore, the time evolution of the shoreline position $s(t)$ is also unknown and must be determined as part of the solution. To deal with this moving boundary problem, we will proceed as follows. First, guided by earlier work on Stefan problems [see *Crank*, 1984] and Gilbert deltas [*Voller et al.*, 2004; *Capart et al.*, 2007], we will assume that the shoreline moves according to the relation

$$s(t) = \lambda\sqrt{D_1 t}, \tag{38}$$

where λ is a nondimensional constant governing the rate of advance of the shoreline into the lake. Assuming then that the evolving shoreline position is known, we will solve separately for the topset and foreset profile evolutions $z_1(x, t)$ and $z_2(x, t)$, subject to the boundary conditions (34)–(36). Finally, we will use the compatibility equation (37) at the shoreline to determine the value of the constant λ and check a posteriori that the assumption (38) for the shoreline speed does indeed generate a valid solution of the overall problem.

[29] Following *Voller et al.* [2004] and *Capart et al.* [2007], we assume for the topset profile evolution the similarity form

$$\frac{z_1(x,t)}{\sqrt{D_1 t}} = f_1(\sigma_1), \tag{39}$$

where $\sigma_1 = \frac{x}{\sqrt{D_1 t}}$. In other words, the topset bed is expected to adopt a self-similar profile, governed by the shape function $f_1(\sigma_1)$ and by a time-varying spatial scale $\sqrt{D_1 t}$ that sets the pace at which the shape is stretched. Note how the vertical elevation z_1, horizontal coordinate x, and shoreline position s evolve according to the same stretching rate, proportional to the square root of time. After substitution of ansatz (39) and repeated application of the chain rule, the diffusion partial differential equation (31) reduces to the ordinary differential equation

$$f_1'' + \frac{1}{2}\{\sigma_1 f_1' - f_1\} = 0, \tag{40}$$

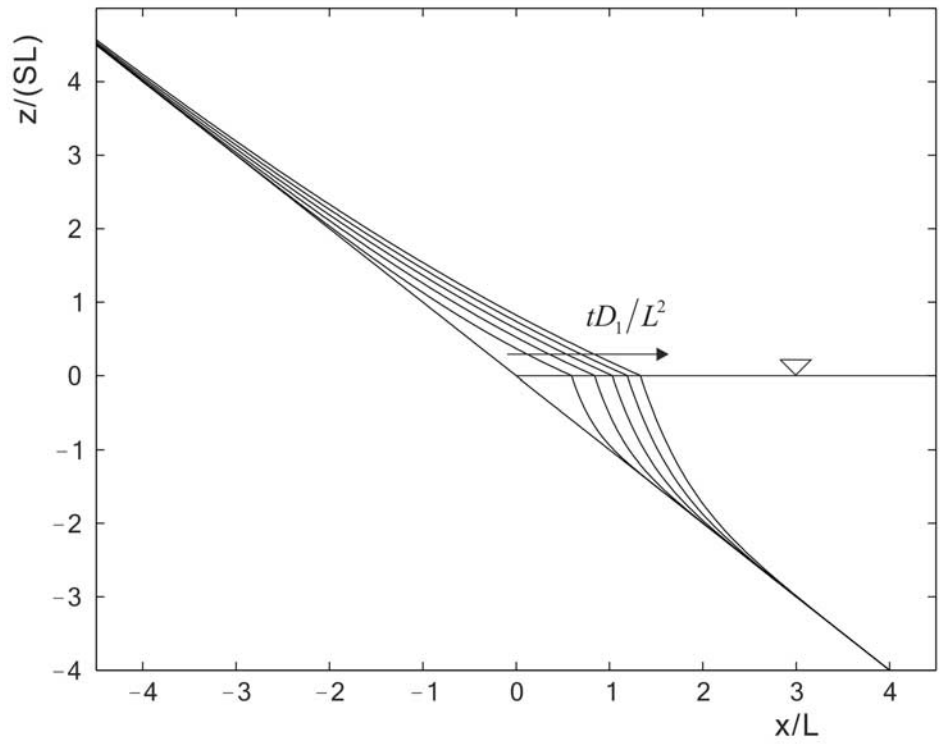

Figure 5. Similarity solution for hyperpycnal delta starting from a constant-slope bed of infinite extent upstream and downstream of the initial shoreline. Delta profiles plotted at equally spaced dimensionless times $tD_1/L^2 = 0, 1, 2, 3, 4, 5$.

where $f_1' = df_1/d\sigma_1$ and $f_1'' = d^2f_1/d\sigma_1^2$. Likewise, the boundary conditions (34) and (36), applied respectively far upstream and at the shoreline (where $\sigma_1 = \lambda$), become

$$f_1'(-\infty) = -S \quad \text{and} \quad f_1(\lambda) = 0. \tag{41}$$

The general solution of equation (40) can be written [for a detailed derivation, see *Capart et al.*, 2007]

$$f_1(\sigma_1) = -A_1\sigma_1 + B_1\left\{2\exp\left(-\sigma_1^2/4\right) + \sigma_1\sqrt{\pi}[\mathrm{erf}(\sigma_1/2) + 1]\right\}, \tag{42}$$

where functions "exp" and "erf" are the exponential and error functions, respectively. Constants A_1 and B_1 are determined on the basis of the applied boundary conditions (41), yielding

$$A_1 = S\ , \quad B_1 = \frac{S\lambda}{2\exp\left(-\lambda^2/4\right) + \lambda\sqrt{\pi}[\mathrm{erf}(\lambda/2) + 1]}. \tag{43}$$

Likewise, along the foreset, we assume the similarity form

$$\frac{z_2(x,t)}{\sqrt{D_2 t}} = f_2(\sigma_2), \tag{44}$$

where $\sigma_2 = \frac{x}{\sqrt{D_2 t}}$. The corresponding solution is written

$$f_2(\sigma_2) = -A_2\sigma_2 + B_2\{2\exp\left(-\sigma_2^2/4\right) + \sigma_2\sqrt{\pi}[\mathrm{erf}(\sigma_2/2) - 1]\}, \tag{45}$$

and the application of boundary conditions (35) and (36) far downstream and at the shoreline (where one must be careful to notice that $\sigma_2 = \lambda\sqrt{D_1/D_2}$) yields for constants A_2 and B_2

$$A_2 = S,$$

$$B_2 = \frac{S\lambda\sqrt{D_1/D_2}}{2\exp\left(-\frac{1}{4}\lambda^2 D_1/D_2\right) + \lambda\sqrt{\pi D_1/D_2}\left[\mathrm{erf}\left(\frac{1}{2}\lambda\sqrt{D_1/D_2}\right) - 1\right]}. \tag{46}$$

At this stage, the whole solution is determined except for the value of constant λ. This is obtained by invoking internal boundary condition (37), which requires a continuous sediment transport rate at the shoreline. In terms of shape functions f_1 and f_2, the condition $q_1 = q_2$ at $x = s(t)$ can be formulated as

$$D_1\{-f_1'(\lambda) - S_{\min,1}\} = D_2\{-f_2'\left(\lambda\sqrt{D_1/D_2}\right) - S_{\min,2}\}. \tag{47}$$

This is a transcendental equation for unknown λ, which depends on the three ratios D_2/D_1, $S_{\min,1}/S$ and $S_{\min,2}/S$. While the equation is too complicated to be solved algebraically, the root λ is easy to determine by numerical means (using for instance Newton iterations), once values are chosen for the control parameters.

[30] Results for one such choice of control parameters are illustrated in Figure 5. The following values were chosen: $D_2/D_1 = 0.1$, $S_{\min,1} = S_{\min,2} = S_{\min}$ and $S_{\min}/S = 0.2$. The

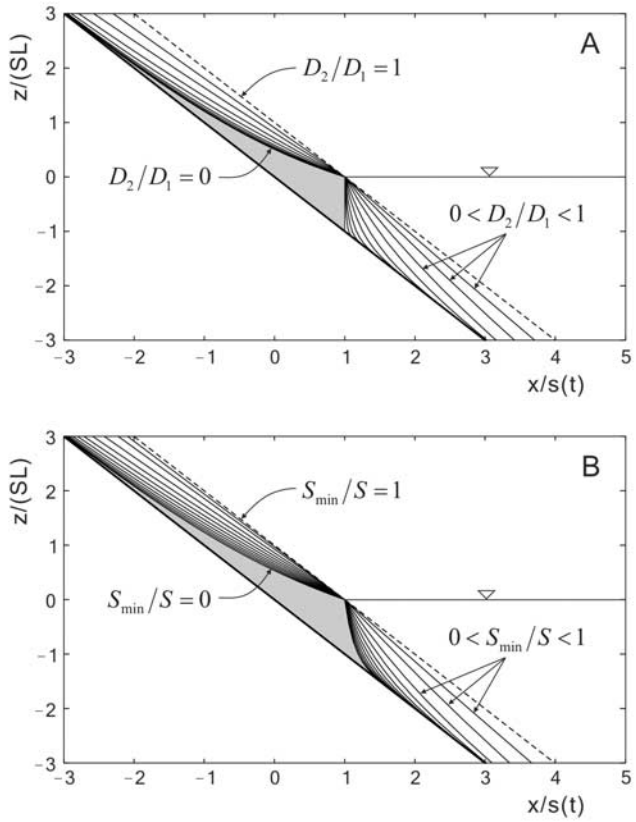

Figure 6. Influence of control parameters on the delta shape: (a) influence of the ratio of foreset to topset diffusion coefficients D_2/D_1, and (b) influence of the ratio of inclination threshold to initial bottom slope S_{min}/S (where $S_{min} = S_{min,1} = S_{min,2}$).

calculated value of root λ for this set of parameters is $\lambda = 0.5957$, and the accuracy of the resulting profiles was insured by checking that conservation of sediment mass is satisfied to more than three significant figures. In Figure 5, the profiles are normalized using an arbitrary length scale L in the horizontal direction x, and a distorted elevation scale SL in the vertical direction z. Successive delta profiles are plotted at equally spaced dimensionless times $tD_1/L^2 = 0$, 1, 2, 3, 4, 5, starting from a bed of constant slope at time $t = 0$. This type of delta growth could occur, for instance, in the years following the damming of a river (as in the case of the Colorado River at Lake Mead), or in the years following a channel diversion (as in the case of the Rhine River at Lake Constance). Two-diffusion solutions having the same general appearance as those of Figure 5 were earlier obtained by *Jordan and Flemings* [1991], using numerical methods.

[31] Like the actual delta profiles in Lake Mead [*Smith et al.*, 1960] and Lake Constance [*Adams et al.*, 2001], the analytical delta solutions depicted in Figure 5 feature concave foresets. The foreset profile is steepest immediately downstream of the shoreline slope break, then decreases in inclination as it descends into the lake, trending asymptotically toward the original bottom slope. Upstream of the shoreline, the river profile is raised above the original bottom, likewise featuring an upward curvature that approaches the original bottom slope far upstream of the delta. This topset shape is analogous to the one derived by *Capart et al.* [2007] for Gilbert-type deltas. For both the subaerial topsets and subaqueous foresets, the bed inclinations along any given ray radiating from the origin stay constant in time. This is because the self-similar shape of the profile is rescaled at the same rate in the x and z directions.

[32] For the calculations of Figure 5, experimental observations (see section 4) were used to guide the choice of parameters. In Figure 6, we illustrate how varying these parameters influences the delta morphology. To highlight shape changes, the profiles shown are normalized with respect to the evolving shoreline position $s(t)$ instead of the constant length L used earlier. In Figure 6a, normalized profiles are plotted for different values of the ratio of foreset to topset diffusion coefficients D_2/D_1. Here the ratio S_{min}/S is set equal to 0.5. Upon varying the ratio of diffusion coefficients in the range $0 \leq D_2/D_1 \leq 1$, delta shapes change from sharply to weakly cusped at the shoreline break. The two end-members of the family of curves plotted in Figure 6 are of interest. When $D_2/D_1 = 0$, subaqueous diffusion is entirely suppressed, and a vertical foreset is obtained. Relative to the distance $s(t)$ between the origin and the shoreline, the delta is most compact in this limit. The other limiting case is obtained when $D_2/D_1 = 1$. If the subaerial and subaqueous diffusion processes are equally strong, then no change of transport capacity occurs at the shoreline, and the bed retains its original flat equilibrium profile. Varying the ratio D_2/D_1 between 0 and 1 yields shapes that gradually flatten both upstream and downstream of the shoreline.

[33] In Figure 6b, the influence of the ratio of inclination threshold to initial bottom slope S_{min}/S is examined, for a constant value of $D_2/D_1 = 0.1$. As the ratio S_{min}/S is varied from 0 to 1, the delta appearance gradually changes from one limiting case to another. When $S_{min}/S = 0$, no inclination threshold is present, yielding a clinoform with gracefully curved topsets and foresets, closely resembling the earlier calculations of *Jordan and Flemings* [1991]. As the inclination threshold rises, both the topset and foreset profiles become closer to straight lines, until $S_{min}/S = 1$ and transport is suppressed. With sediment transport deactivated both upstream and downstream of the shoreline, the bottom keeps its original constant inclination profile.

[34] Qualitatively, the shape variants obtained by modifying either D_2/D_1 or S_{min}/S are seen in Figures 6a and 6b to be rather analogous to each other. It would thus appear like a case of equifinality [see, e.g., *Schumm*, 1991], in which different combinations of parameters associated with different physical mechanisms could account equally well for a given delta morphology. One would then doubt the necessity of invoking inclination thresholds in addition to the effect of contrasting diffusion strengths. Equifinality is not encountered in this case, however, because the two parameter ratios have a different influence on the rate of advance of the shoreline. Used in Figure 6 to normalize the profiles, the shoreline position history $s(t)$ is itself an observable that must be accounted for by the theory, and this observable does respond differently to different combinations of parameters.

[35] The influence of parameter values on shoreline speed is illustrated in Figure 7, which shows a contour map of the dimensionless rate of shoreline advance, $\lambda = s(t)/\sqrt{D_1 t}$, as a

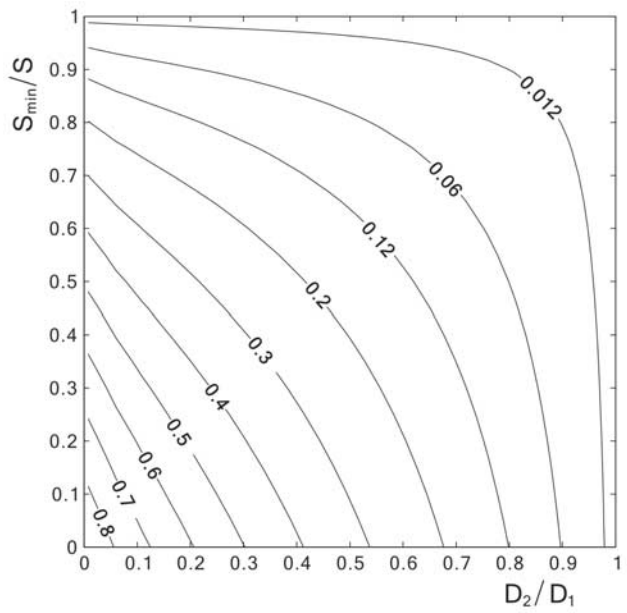

Figure 7. Influence of ratios D_2/D_1 and S_{min}/S on the dimensionless rate of shoreline advance $\lambda = s(t)/\sqrt{D_1 T}$, for a hyperpycnal delta of infinite extent upstream and downstream.

function of ratios D_2/D_1 and S_{min}/S. Two limiting cases are again of interest. The fastest shoreline advance is observed at the origin of the map ($D_2/D_1 = 0$ and $S_{min}/S = 0$), where the delta shape is most compact. This corresponds to a semi-infinite diffusional delta topset with vertical foreset, for which $\lambda = 0.9034$. Along the right margin ($D_2/D_1 = 1$) and the top margin of the map ($S_{min}/S = 1$), on the other hand, no delta deposit forms and the shoreline does not advance ($\lambda = 0$). In between these two limiting cases, the rate of shoreline advance responds differently to the two control parameters: it decreases linearly with respect to ratio S_{min}/S along axis $D_2/D_1 = 0$, and nonlinearly with respect to ratio D_2/D_1 along axis $S_{min}/S = 0$. Our experience in calibrating these parameters to fit data from laboratory tests (see section 4) is that only one combination of values yields results that best approximate both the delta shape and the rate of shoreline advance.

[36] A second simple geometry for which similarity solutions can be derived is illustrated in Figure 4b. This case differs from case A described earlier in the choice of upstream boundary conditions. Instead of extending infinitely far upstream, the topset here has a finite extent, with a prescribed sediment influx imposed at the origin $x = 0$. Like case A, the initial condition is a lake bed of constant inclination or, equivalently, a lake of linearly varying depth, extending infinitely far downstream. We again assume a constant water level in the lake. The corresponding mathematical problem is the same as before, except for the domain of the topset and its upstream boundary condition. Equations (31) and (34) become

$$\frac{\partial z_1}{\partial t} - D_1 \frac{\partial^2 z_1}{\partial x^2} = 0, \ 0 < x < s(t) \tag{48}$$

and

$$q_1 = D_1\left(-\partial z/\partial x - S_{min,1}\right) = I, \ x = 0, \tag{49}$$

where I is the prescribed volumetric sediment influx (per unit width) at the origin. The other equations of set (31)–(37) remain applicable. A practical example leading to this situation would be a silted check dam positioned at the upstream edge of a reservoir.

[37] The solution procedure follows the same lines as before. Again, the rate of advance of the shoreline is assumed to take the form $s(t) = \sqrt{D_1 t}$, where the value of dimensionless constant λ will have to be determined anew. The solution for the topset takes the similarity form (39), but now the shape function $f_1(\sigma_1)$ is written

$$f_1(\sigma_1) = -A_1\sigma_1 + B_1\{2\exp\left(-\sigma_1^2/4\right) + \sigma_1\sqrt{\pi}\,\mathrm{erf}(\sigma_1/2)\}. \tag{50}$$

Its derivative at the origin is

$$f_1'(0) = -A_1, \tag{51}$$

and it follows from the upstream boundary condition (49) that

$$A_1 = \frac{I}{D_1} + S_{min,1}. \tag{52}$$

Constant B_1 is then obtained by requiring $f_1(\lambda) = 0$, yielding

$$B_1 = \frac{A_1\lambda}{2\exp\left(-\lambda^2/4\right) + \lambda\sqrt{\pi}\,\mathrm{erf}(\lambda/2)}. \tag{53}$$

The solution for the foreset is exactly the same as before, and equation (47) expressing continuity of the sediment transport at the shoreline remains applicable. Because the topset function $f_1(\sigma_1)$ has changed, however, the value of root λ is also affected. Furthermore, a new control parameter I/D_1S intervenes in addition to parameter ratios D_2/D_1, $S_{min,1}/S$, and $S_{min,2}/S$. The solution example presented in Figure 8b corresponds to the following values: $I/D_1S = 3$, $D_2/D_1 = 0.1$, and $S_{min,1}/S = S_{min,2}/S = 0.2$, yielding for the root λ the value $\lambda = 1.375$.

[38] The third geometry considered is illustrated in Figure 4c. A lake of constant depth H_0 is assumed, extending over domain $0 < x < \infty$, with a prescribed bed elevation Z_0 at the origin. This is a sedimentary analogue of the classical two-phase Stefan problem [see *Crank*, 1984] describing the propagation of a melting front. The mathematical problem for this case is, in full,

$$\frac{\partial z_1}{\partial t} - D_1 \frac{\partial^2 z_1}{\partial x^2} = 0, \ 0 < x < s(t) \tag{54}$$

$$\frac{\partial z_2}{\partial t} - D_2 \frac{\partial^2 z_2}{\partial x^2} = 0, \ s(t) < x < \infty \tag{55}$$

$$z = -H_0, \ 0 < x < \infty, \ t = 0 \tag{56}$$

$$z_1 = Z_0, \ x = 0, \tag{57}$$

$$z_2 = -H_0, \ x \to \infty \tag{58}$$

$$z_1 = z_2 = 0, \quad x = s(t) \tag{59}$$

$$q_1 = q_2, \quad x = s(t). \tag{60}$$

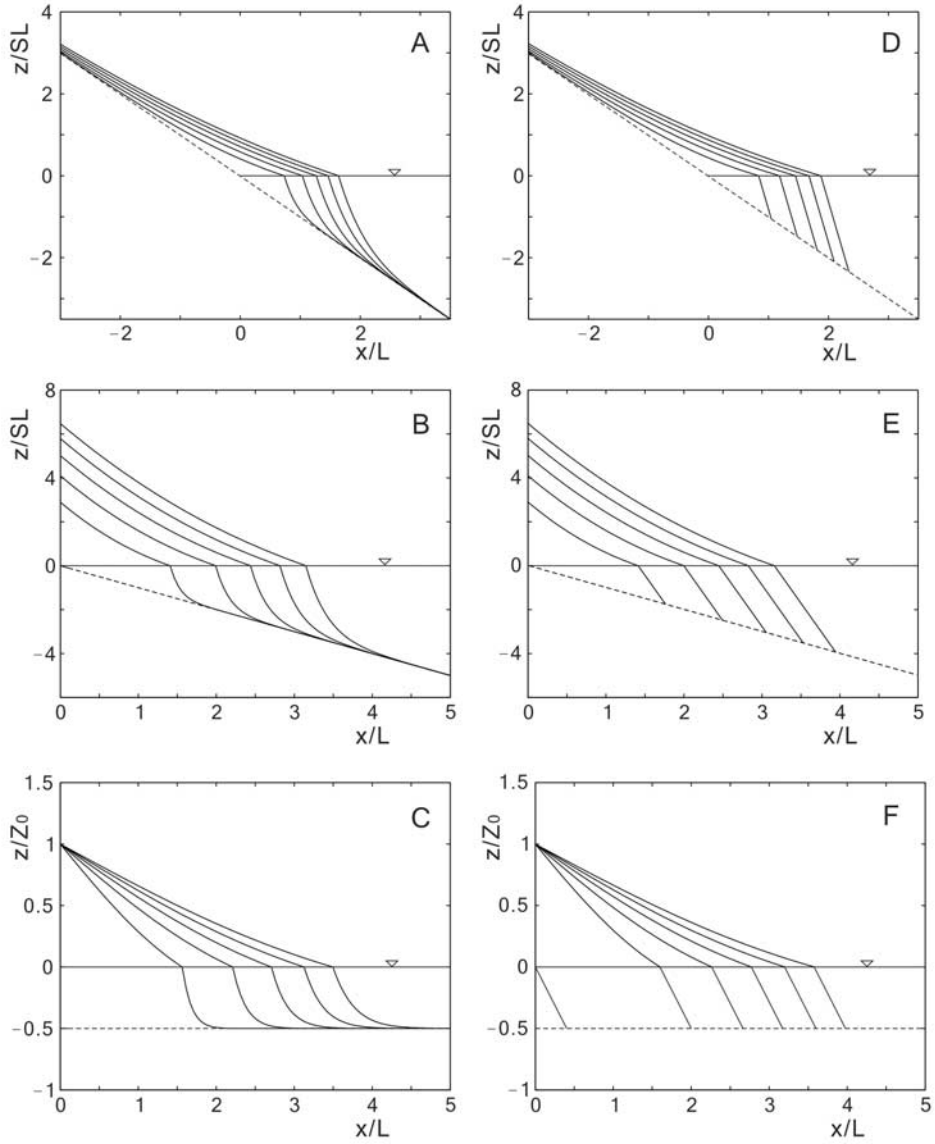

Figure 8. Similarity solutions for (left) hyperpycnal and (right) Gilbert deltas: (a) hyperpycnal delta of infinite extent; (b) hyperpycnal delta with finite topset; (c) hyperpycnal delta in lake of constant depth, mathematically equivalent to the two-phase Stefan problem with zero latent heat; (d) Gilbert-type delta with semi-infinite topset [*Capart et al.*, 2007]; (e) Gilbert delta with finite topset [*Voller et al.*, 2004]; and (f) Gilbert delta in lake of constant depth, mathematically equivalent to the single-phase Stefan problem [see *Crank*, 1984]. Delta profiles plotted at equally spaced dimensionless times $tD_1/L^2 = 0, 1, 2, 3, 4, 5$.

The expression for the shoreline is again $s(t) = \lambda\sqrt{D_1 t}$. In this geometry, however, the similarity forms for the topset and foreset evolution become

$$\frac{z_\alpha}{Z_0} = f(\sigma_\alpha),\ \sigma_\alpha = x/\sqrt{D_\alpha t},\ \alpha = 1, 2, \tag{61}$$

and it is required that $S_{\min,1} = S_{\min,2} = 0$ for strict similarity to be met. Here the delta shape is stretched over time only in the x direction, keeping the same scale Z_0 in the z direction. The analytical solution of this problem is well known: it coincides with the Neumann solution of the two-phase Stefan problem [see *Crank*, 1984], in the special case of a zero latent heat. A detailed derivation following the same lines as the solutions for cases B and C is provided in *Lai* [2006]. Solution profiles are illustrated in Figure 8c, for the following values of the control parameters: $Z_0/H_0 = 2$, and $D_2/D_1 = 0.1$. The associated value of root λ is $\lambda = 1.563$. In contrast with case C, the hyperpycnal delta problems A and B have no obvious analogues in the theory of heat transfer, and our analytical solutions for these cases appear to be new.

[39] It is instructive to compare the hyperpycnal delta solutions for cases A, B, and C with each other, and to contrast them with the corresponding solutions for Gilbert-type deltas. The resulting plots are presented in synoptic

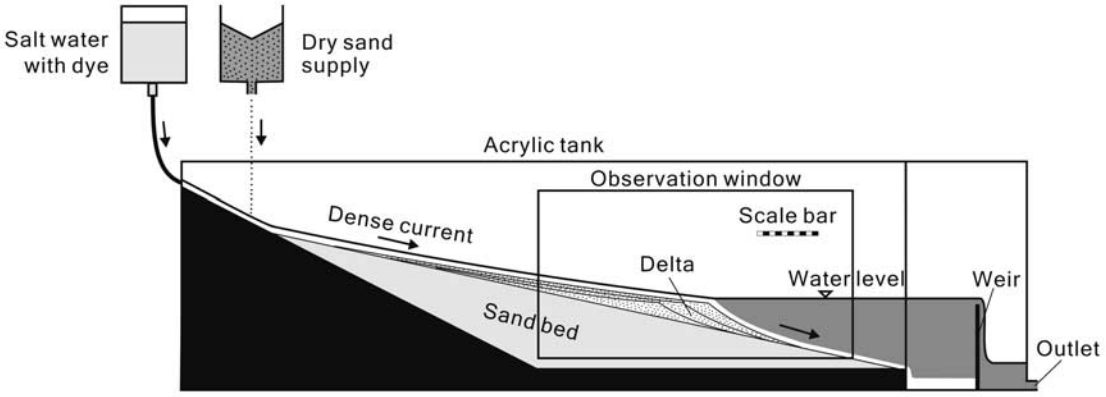

Figure 9. Experimental setup used for the small-scale laboratory experiments.

form in Figure 8. The left plots, Figures 8a, 8b, and 8c, feature hyperpycnal delta profiles evolving according to our two-diffusion description, involving the joint geomorphic action of a river flow and its associated turbidity underflow. The right plots, on the other hand, Figures 8d, 8e, and 8f, show Gilbert-type deltas evolving under a combination of subaerial alluvial diffusion and subaqueous angle-of-repose avalanching. These were plotted using the analytical solutions documented by *Voller et al.* [2004] and *Capart et al.* [2007].

[40] The most obvious differences between the left and right columns of Figure 8 concern the morphology of the delta foresets. The hyperpycnal deltas have gently curved foresets which trend smoothly toward the original lake bottom at the downstream end. The Gilbert deltas, on the other hand, feature straight foresets with a sharp slope break at the downstream toe. Less obviously, the foreset shapes have an influence on the progradation rates of the deltas. The corresponding control parameters are, respectively, the ratio of diffusion constants D_2/D_1 for the hyperpycnal deltas, and the ratio of foreset inclination to initial slope R/S for the Gilbert deltas. These parameters, however, can be tuned to yield the same rates of advance for curved and straight foresets. Furthermore, the shape functions for the topsets are identical, regardless of the assumed foreset morphology. An important implication is that the foreset shape cannot be ascertained only on the basis of topset and shoreline measurements, using for instance data from airborne photogrammetry. To determine foreset morphology, a bathymetric survey is required.

[41] Overall, hyperpycnal and Gilbert-type deltas also present a number of resemblances. Their topsets have similar shapes, and they both exhibit a sharp slope break at the shoreline. There the bed load sediment dumped at the river mouth aliments the foreset buildup and drives the delta progradation. In both cases, symmetries of the diffusion equation lead to the existence of similarity solutions, under special choices of initial and boundary conditions. In the next section, we will compare the similarity solutions to the results of small-scale laboratory experiments.

4. Experiments and Comparison

[42] To test the theory and computations described in the previous sections, small-scale laboratory experiments were conducted at the Hydrotech Research Institute of the National Taiwan University. The apparatus used for this purpose, illustrated in Figure 9, is a small-scale version of the experimental setup developed by *García* [1993] for the study of turbidity currents. The flows of interest take place in a narrow flume having the following dimensions: width = 1 cm; length = 100 cm; height = 40 cm. Upstream, the flume is supplied with both liquid and sediment. An elevated medical pouch is used to supply a steady liquid discharge at the upstream end of the flume. The supplied liquid is a brine solution of homogeneous density, prepared by thoroughly mixing tap water with dissolved salt. A bit further downstream, dry sand is supplied using a small silo placed above the flume. The silo releases a steady stream of sand grains onto distributor plate vibrated using an eccentric mass rotated by a small electric motor. The properties of the sand material and brine solution used are summarized in Table 1. For background regarding the sand properties and their mode of measurement, the reader is referred to *Das* [1990]. For each experiment, the brine discharge is estimated by timing the volume outflow.

[43] At the downstream end of the flume, the narrow channel expands into a wide receiving tank of length and width equal to 20 by 20 cm. The tank is deeper than the bottom of the narrow channel in order to collect exiting density currents under free outfall conditions. The water level in the tank is controlled by a rigid weir, over which the water discharges to the outlet.

[44] Prior to conducting an experiment, a sediment bed having a constant inclination of approximately 10 degrees is first prepared, by running the flume under steady supply of brine and sand, with the lake kept dry. The flume is operated in this fashion until the bed has approached its equilibrated,

Table 1. Properties of the Sand Material and Brine Solution Used for the Experiments

Property	Value
Median sand diameter d_{50}, mm	0.17
Sand uniformity coefficient $C_u = d_{60}/d_{10}$	2.3
Sand density ρ', g/cm^3	2.67
Porosity of uncompacted sand bed $n_0 = V_{voids}/V$	0.507
Angle of repose φ, deg	37
Upstream brine density ρ_1, g/ml	1.20
Water density in receiving ambient ρ_∞, g/ml	1.00

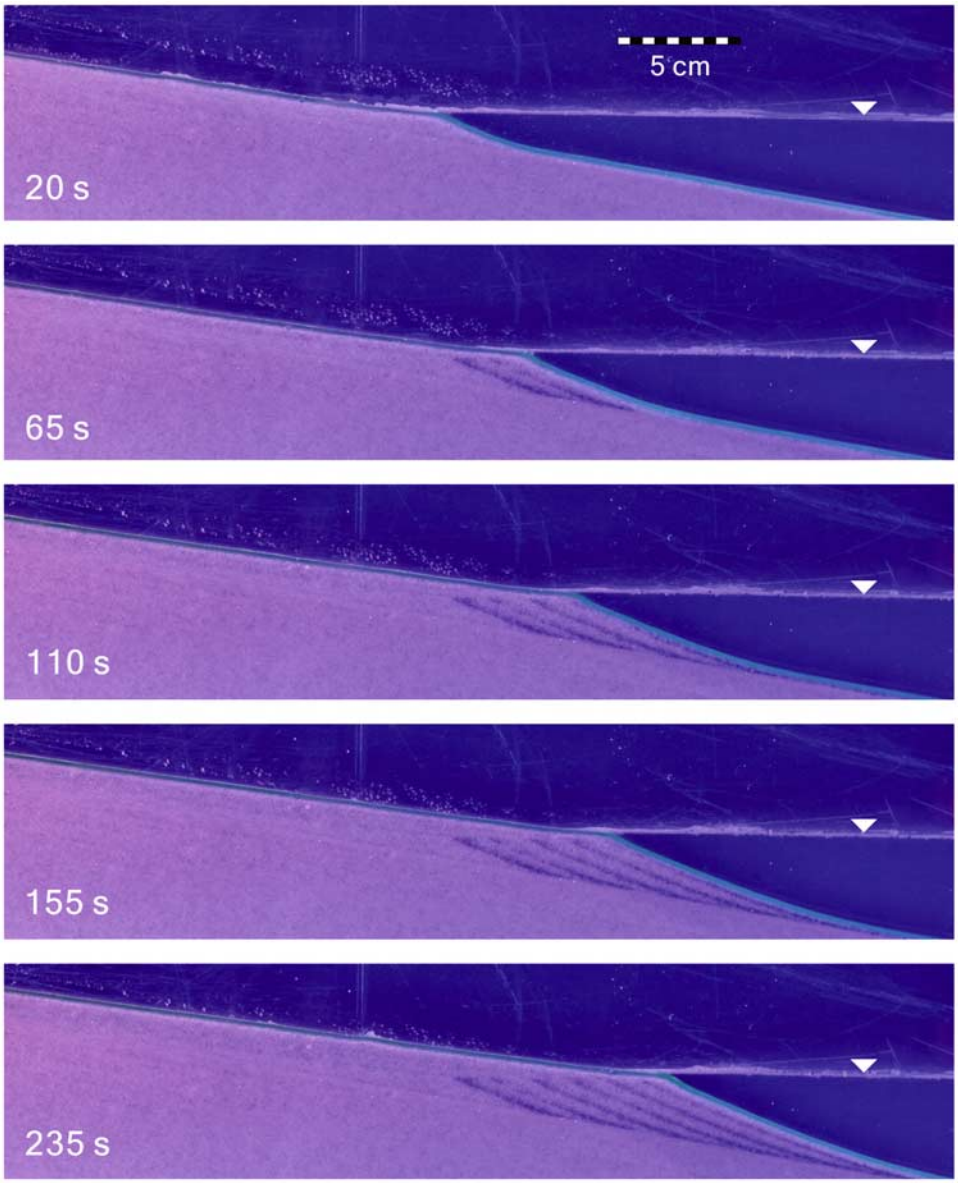

Figure 10. Series of experimental photographs depicting the progradation of a hyperpycnal delta in a lake of constant water level, starting from a bed profile of constant inclination. See text for a detailed interpretation.

constant slope profile, a process which takes about 3 to 5 min when started from a bed that was first roughly profiled by hand (for an analysis of this equilibration process, see *Capart et al.* [1998]). When the desired starting conditions are attained, the downstream lake level is rapidly raised to its desired height, by feeding water into the receiving tank using the secondary supply. No adjustments are made to the upstream supply of brine and sand, which continue to operate under the conditions used to equilibrate the bed. This procedure is an adapted version of the procedure proposed by *Bellal et al.* [2003] to study prograding Gilbert deltas.

[45] The ensuing delta evolution is monitored using time-lapse photography. For this purpose, a professional digital camera mounted rigidly on a tripod is used to image the flow through the transparent flume sidewalls at precisely timed intervals of 5 s. The observation window is centered on the channel reaches immediately upstream and downstream of the evolving shoreline. Various means are used to facilitate visualization. First, fluorescent dye is mixed with the brine solution, and illuminated using black (UV) light. The resulting greenish subaerial and subaqueous brine currents contrast sharply with the dark background, the clear ambient water of the lake, and the underlying sediment bed. To visualize the internal stratigraphy of the delta, furthermore, coal ashes can be sprinkled upstream of the observation section, which thereafter get trapped inside the foreset deposits. There the ashes form dark stripes which contrast well with the brighter sand grains.

[46] The bed elevation profile, position of the shoreline, and the lake level height are extracted semimanually from each digital photo using mouse clicks. Pixel positions are then converted to physical coordinates using a calibrated linear transformation. To permit this calibration, a scale bar is placed in the field of vision, and a photo of a horizontal

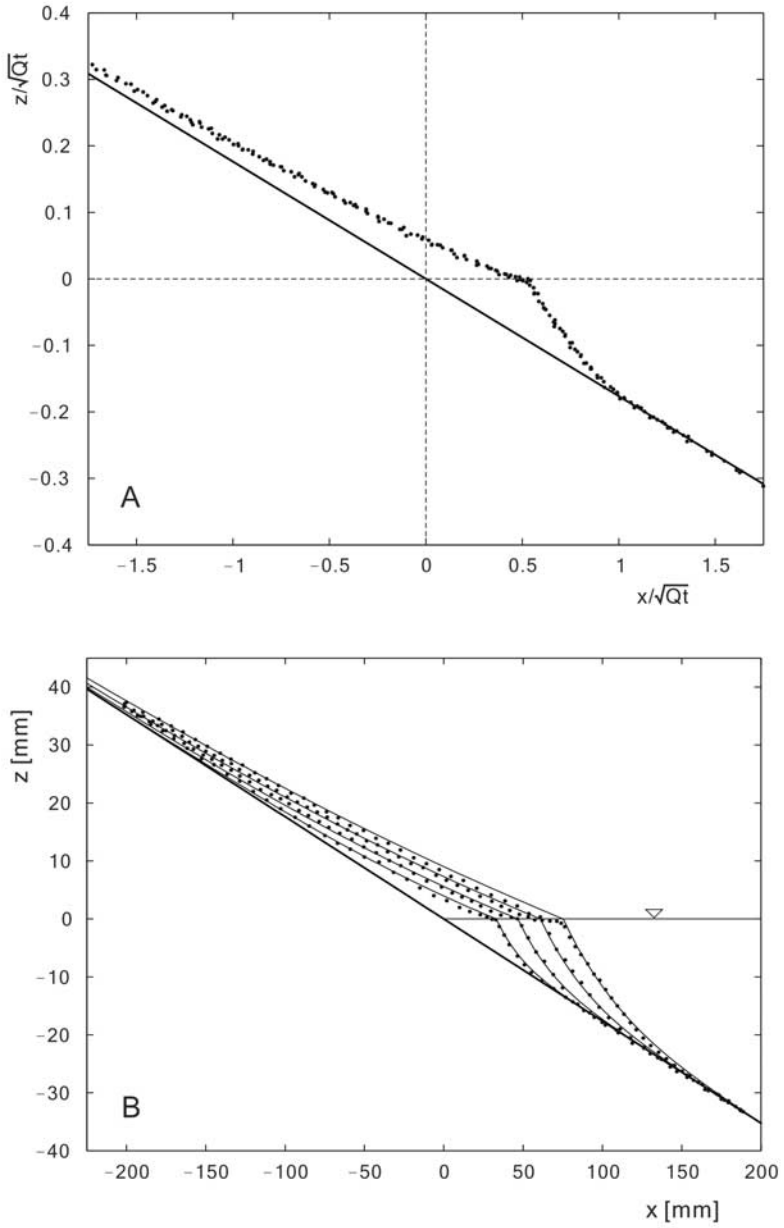

Figure 11. Results for hyperpycnal delta progradation under the lower brine influx $Q = 1.54 \times 10^2$ mm^2/s (run 1): (a) measured bed profile data scaled by the inverse square root of the elapsed time t and (b) comparison of measured data (dots) and analytical solution (lines). Profiles for run 1 in Figures 11a and 11b are sampled at times t = 20, 45, 80, 125 s.

level is taken prior to the experiments to determine precisely the reference horizon. Our time-lapse photography approach is inspired from the approach used by *Muto* [2001] and *Muto and Swenson* [2005] for their small-scale Gilbert delta experiments. More details about the laboratory setup and image analysis procedures used in the present work can be found in work by *Lai* [2006].

[47] Two runs are selected for quantitative comparisons with the two-diffusion theory. Both are conducted under constant lake level, with sufficient channel lengths upstream and downstream of the initial shoreline to approximate semi-infinite topset and foreset beds. The initial slopes and brine densities in both cases are the same, and the two runs differ only by the value of the salt water discharge supplied upstream of the channel. Run 1 is conducted under a lower brine influx Q = 154 mm^2/s (discharge divided by channel width), while run 2 is conducted under the higher brine influx Q = 229 mm^2/s.

[48] Before looking at quantitative comparisons, it is useful to first describe experimental observations. For this purpose, a sequence of photographs acquired during run 1 is shown in Figure 10. The time-stamped photos record side views of the delta buildup, under conditions of steady upstream inflow and constant downstream lake level, marked by the inverted white triangles in Figure 10. Made visible by the green fluorescent dye, the shallow layer of

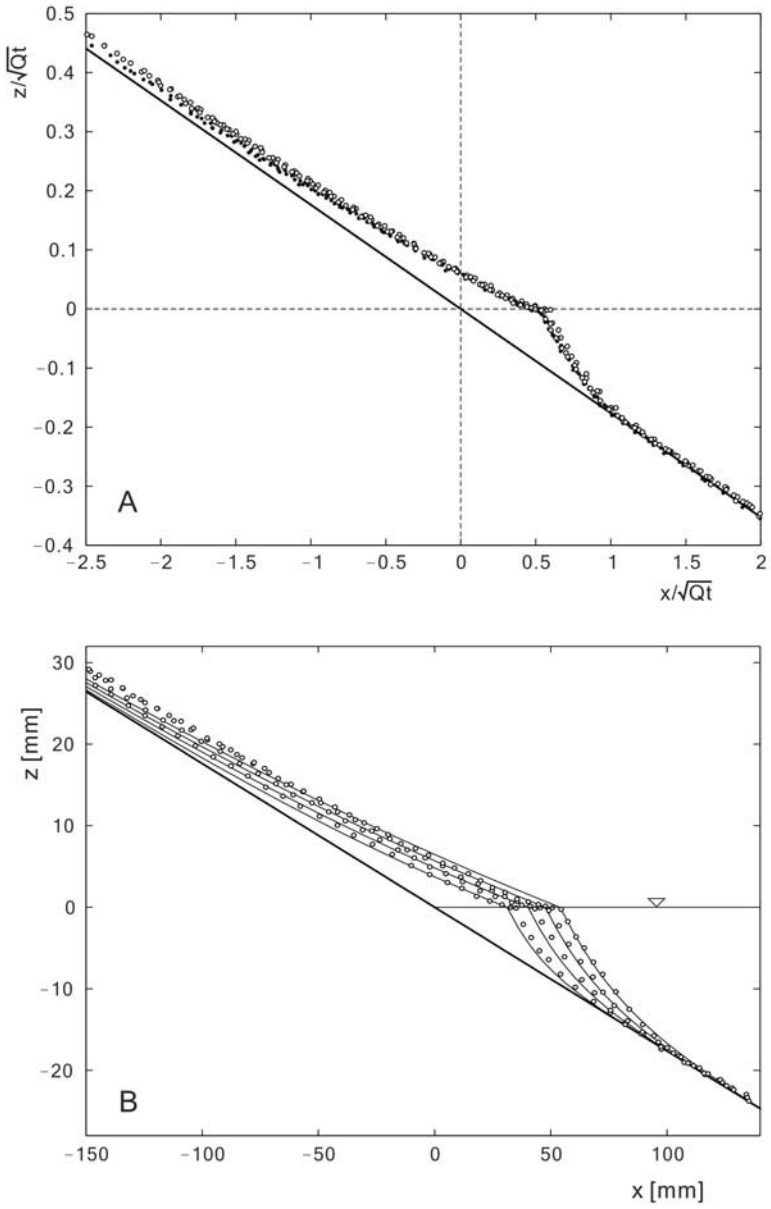

Figure 12. Hyperpycnal delta progradation under different brine discharges: (a) results for the higher brine influx $Q = 229$ mm^2/s (run 2, circles) plotted together with the results for the lower brine influx $Q = 154$ mm^2/s (run 1, dots), upon scaling by the inverse square root of the integrated brine flux Qt and (b) comparison of measured data (circles) and analytical solution (lines) for run 2. The profiles for run 2 in Figures 12a and 12b are sampled at times $t = 20, 30, 40, 50$ s.

dense brine flows from left to right along the sediment deposit. The current is subaerial upstream, then plunges into the lake at the shoreline break, continuing its course as a subaqueous underflow. Under the geomorphic action of the hyperpycnal flow, the delta progrades lakeward, simultaneously building up topset and foreset deposits on both sides of the shoreline.

[49] The observed morphology closely resembles the profiles predicted by the two-diffusion theory (see Figure 5), and is qualitatively similar to the Rhine delta profile at Lake Constance depicted earlier in Figure 1. Both the topset and foreset are concave upward, and everywhere gently curved except for the sharp cusp at the shoreline break, with the topset curvature milder than the foreset curvature. The maximum inclination of the foreset is approximately 24 degrees, well below the measured angle of repose of 37 degrees (see Table 1). At its toe, the foreset connects smoothly with the original lake bed, without any conspicuous break of slope at its leading edge. Delta profiles at different times are scaled versions of each other, consistent with the expected self-similar growth. This is further reflected by the internal bedding, made visible by the dark ash stripes trapped in the foreset deposits. A geometrically self-similar stratigraphy is thus generated by the self-similar evolution of the delta morphology. The obtained internal

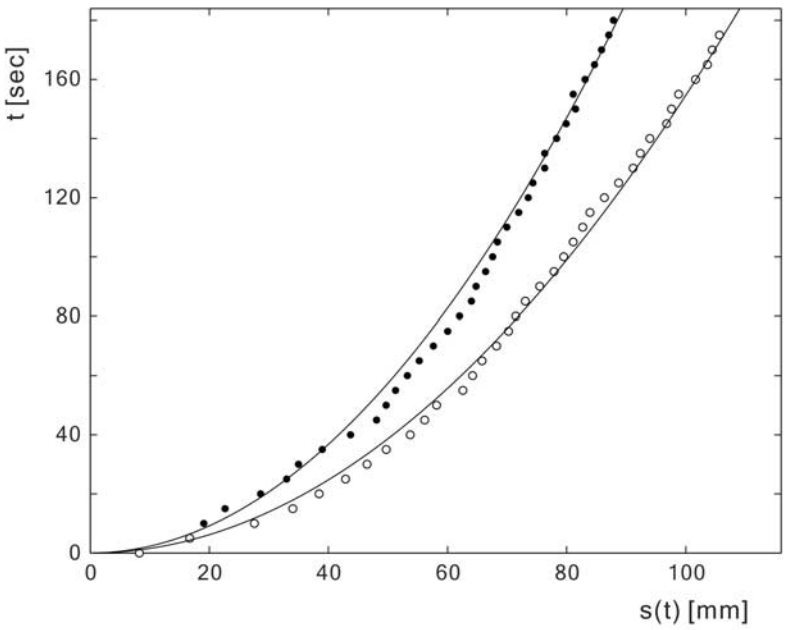

Figure 13. Comparison of experimental and analytical results for the time-varying shoreline position of hyperpycnal deltas: dots, measured results for the lower brine influx Q = 154 mm^2/s (run 1); circles, measured results for the higher brine influx Q = 229 mm^2/s (run 2); lines, analytical shoreline paths.

architecture resembles the stratigraphy of field-scale clinoforms described by *Posamentier and Allen* [1999].

[50] The experimental profiles can now be used to assess quantitatively the two-diffusion theory derived in the previous sections. One implication of the theory that can be checked without recourse to the analytical solutions is the predicted self-similarity of the delta evolution. When both the x and z coordinates of the bed profiles are measured with respect to the original position of the shoreline, and scaled by the inverse square root of the elapsed time, profiles observed at different times during a single experiment should collapse together. For run 1, this is verified in Figure 11a, where measured delta profiles from 4 different times (t = 20, 45, 80, and 125 s) are plotted together in the reduced coordinates $x/\sqrt{Qt}$, $z/\sqrt{Qt}$. Self-similarity is found to be well approximated for at least the first two minutes of the delta buildup. Because the experimental channel has a finite length instead of the infinite extent assumed by the analytical theory, however, later profiles gradually drift away from geometric self-similarity.

[51] In Figure 11b, the same profiles are compared with the analytical solutions derived in section 3. Calculations are performed using the experimental values listed in Table 1 for the densities ρ_1 (brine influx), ρ' (sand material) and ρ_∞ (receiving water ambient), and for the bed porosity n_0, and friction angle φ. The remaining parameters for which values are needed are the dimensionless velocity coefficients α_1 and α_2, and inclination threshold $S_{\min}$. These are calibrated on the basis of the delta profile at time t = 125 s, yielding values

$$\alpha_1 = 0.59, \quad \alpha_2 = 0.30, \quad S_{\min}/S = 0.4. \tag{62}$$

For run 1 (Q = 154 mm^2/s), the corresponding diffusion coefficients D_1 and D_2 along the topset and foreset take the values

$$D_1 = 199 \text{ mm}^2/\text{s}, \quad D_2 = 16.9 \text{ mm}^2/\text{s}. \tag{63}$$

Across the shoreline, the estimated reduction in diffusivity $D_2/D_1 \approx \frac{1}{12}$ is thus about twice as strong (due to factor $\alpha_2/\alpha_1 \approx \frac{1}{2}$) as the reduction in excess density $(\rho_1 - \rho_\infty)/\rho_1 = \frac{1}{6}$. For these parameters, the calculated value of root λ is $\lambda = 0.468$. Without including an inclination threshold (i.e., setting $S_{\min} = 0$), the qualitative morphology of the delta could be reproduced, but quantitative agreement would be significantly reduced. By contrast, little is gained by tuning separately the two slope thresholds $S_{\min,1}$ and $S_{\min,2}$ along the topset and foreset. These conclusions may of course be tied to the specific conditions of the present small-scale experiments, and may not carry over to larger-scale experiments, let alone field cases.

[52] As demonstrated by the profiles of Figure 11b, the analytical solution is found to provide a good approximation of the measured delta profiles. The morphology of the topset and foreset, as well as the pace of the delta buildup and shoreline advance are accurately reproduced by the theory. Deviations are however observed for the topset profile immediately upstream of the shoreline. Whereas the analytical profiles are inclined throughout the topset, the experimental profiles exhibit a nearly horizontal platform in this region. This may be due to local deviations from the normal flow regime assumed in the present theory.

[53] A stronger test of the theory can be carried out by comparing results from run 1 with those of run 2. For this second run, the rate of brine inflow Q was increased from

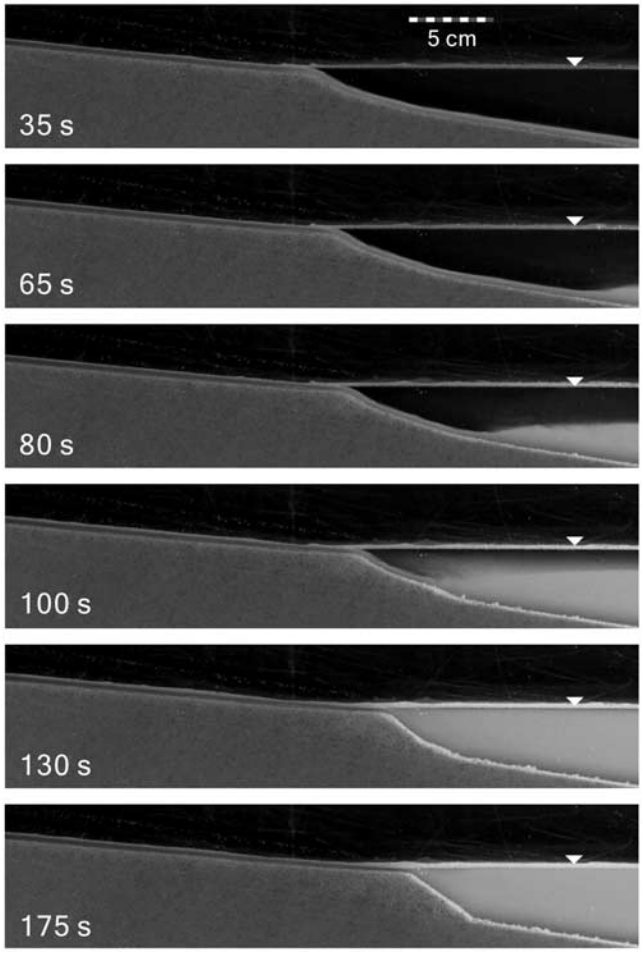

Figure 14. Transition from hyperpycnal to homopycnal (Gilbert-type) delta in small-scale experiments subject to ponding of the brine current (appearing in light gray) at the deep end of the lake.

Q = 154 mm^2/s (run 1), to Q = 229 mm^2/s (run 2), starting again from a bed of identical uniform inclination (10 degrees) and keeping the same brine density. Because relations (13) and (25) for the topset and foreset diffusivities both exhibit a linear dependence on the brine influx Q, the delta profiles for runs 1 and 2 should be geometrically similar to each other when normalized with respect to the square root of the integrated brine flux $\sqrt{Qt}$. To test this implication of the theory, data from the two runs are plotted together in Figure 12a, in the reduced coordinates $x/\sqrt{Qt}$, $z/\sqrt{Qt}$. For run 2, profiles from different times again approximately collapse together. Moreover, the scaled profiles from runs 1 and 2 align rather closely with each other. Similarity between runs conducted under different brine fluxes is thus verified in addition to the self-similarity of a single run over time. This confirms that the anticipated linear dependence of the topset and foreset diffusivities on the brine inflow Q constitutes a reasonable first approximation.

[54] In Figure 12b, the profiles for run 2 are compared with the analytical solutions. For this comparison, the same calibrated values as before are used for parameters α_1, α_2, and S_{min} (see equation (62)). Because the brine inflow Q has changed, however, the diffusivities D_1 and D_2 are higher than before. They now take values D_1 = 295 mm^2/s and D_2 = 25.1 mm^2/s, both increased in proportion to the increase in Q. Because ratios D_2/D_1 and S_{min}/S are the same for both sets of computations, the dimensionless rate of shoreline advance λ = 0.468 stays the same.

[55] As shown in Figure 12b, the analytical solution approximates well the measured profiles for run 2. Agreement is again close for the foreset morphology and pace of delta progradation. Deviations are however registered in the upstream reaches of the topset, where the experimental data rise above the analytical solution. This may be due to an imperfect equilibration between the initial bed slope and the sand supply provided upstream during the experiment. Considering that parameters have not been recalibrated for this second run, the agreement registered is significant and provides some further confidence in the analysis.

[56] In Figure 13, more detailed data for the evolution of the shoreline position are presented, with results from runs 1 and 2 plotted together in dimensional form. The analytical curves and their dependence on the square root of time are seen to provide a reasonable approximation of the observed shoreline paths. As predicted by the theory, the pace of shoreline advance is higher for run 2 than for run 1, in rough proportion to the square root of the increase in brine inflow Q between the two runs. In work by *Lai* [2006], other runs conducted under variable lake level are reported and compared with numerical solutions, yielding a similar degree of agreement.

[57] Although no quantitative analysis will be performed for this run, one final experiment can be presented to highlight the contrast between hyperpycnal and Gilbert-type delta foresets. This experiment, illustrated in Figure 14, was produced by placing a weir at the downstream end of the narrow channel instead of inside the wide receiving tank. This has the effect of reducing considerably the storage volume of the lake. As a result, the dense brine underflow rapidly pools at the deep end of the lake instead of exiting past the free overfall. Eventually, the upper interface of the subaqueous brine pool rises up to the water surface. Because the liquid density in the lake is now equal to the density of the brine supply, the lake inflow switches from hyperpycnal to homopycnal. The resulting delta front rapidly sheds its gently curved morphology to adopt the hallmark angle-of-repose profile of Gilbert-type foresets.

5. Conclusions

[58] In the present work, we sought to derive and test a simple description of the morphological evolution of hyperpycnal deltas. The proposed mechanism involves bed load transport along both the topset and foreset of the delta. Bed load transport is assumed driven by streamflow along the subaerial topset, and by turbid underflow along the subaqueous foreset. By applying the normal flow approximation to both domains, it was shown that the topset and foreset evolutions can both be described by linear diffusion equations. Different diffusivities apply to the subaerial and subaqueous domains, with a diffusivity contrast that is controlled primarily by the relative densities of the turbid water inflow and receiving ambient. Furthermore, both diffusivities are proportional to the turbid water discharge supplied upstream of the delta.

[59] For infinite or semi-infinite channels of uniform initial slopes plunging into lakes of constant water level, it was shown that the corresponding mathematical problem could be solved exactly. To test the implications of the theory, these analytical profiles were then compared with small-scale laboratory experiments. As predicted by the theory, the resulting hyperpycnal deltas adopt self-similar profiles during their progradation. Deltas evolving under different rates of brine inflow are geometrically similar to each other. Also, the experimental profile and shoreline evolutions are well approximated by the analytical solutions.

[60] Finally, an experiment in which the inflow changes from hyperpycnal to homopycnal was presented to highlight the strong influence of relative inflow density on the foreset morphology. Whereas homopycnal inflows lead to avalanching foresets having inclinations close to the angle of repose, with slope breaks at the shoreline and at the foreset toe, hyperpycnal inflows generate concave foresets, which connect smoothly with the lake bathymetry at their distal end. Such concave foresets, predicted by our theory and observed in the present experiments, resemble the subaqueous morphology of natural deltas in lakes known to be prone to turbidity currents. This suggests that bed load transport at the base of dense underflows may shape the morphology of delta foresets in the field as well as in the laboratory.

[61] Nevertheless, caution must be exercised before extrapolating from the present idealized experiments to field cases. Aside from inevitable scale effects, actual hyperpycnal deltas involve sediments that may vary widely in size, and include fines that will settle out of suspension at variable rates. Controls may also be exerted by the detailed flow pattern near the shoreline, or the density stratification of the lake. Moreover, the subaqueous bed material may be set in motion by a variety of processes, including creep and landsliding, or by pulsating currents instead of the sustained underflows assumed in the present work. In the field, it may be difficult to distinguish between these processes on the basis of morphology alone. More reliable conclusions must therefore rely on an analysis of small-scale bathymetric features [*Bornhold and Prior*, 1990], seismic surveys [*Adams et al.*, 2001], in situ underflow measurements [*Best et al.*, 2005], and grain size distributions [*Syvitski and Alcott*, 1993].

Notation

A, B, C constants of integration;
α_1, α_2 dimensionless velocity coefficients;
β local bed inclination;
D_1, D_2 diffusion coefficients along the topset and foreset ($L^2\ T^{-1}$; L is length, T is time);
δ thickness of the bed load layer (L);
exp, erf exponential and error functions;
E entrainment coefficient;
$f(\sigma)$ shape function of self-similar profile;
$f'(\sigma)$, $f''(\sigma)$ first and second derivatives of shape function;
g gravitational acceleration ($L\ T^{-2}$);
φ angle of friction, set equal to the angle of repose;
h depth of the flowing turbid layer (L);
H_0 constant lake depth (L);
λ reduced horizontal coordinate of the moving shoreline;
$\dot{m}$ mass flow rate of the subaerial turbid flow (per unit width) ($M\ L^{-1}\ T^{-1}$; M is mass);
$\dot{m}'$ excess density flux of the subaqueous turbidity current ($M\ L^{-1}\ T^{-1}$);
n_0 sand bed porosity;
$q = q(x, t)$ volume flux of bed load (per unit width) ($L^2\ T^{-1}$);
Q upstream inflow of turbid water (per unit width) ($L^2\ T^{-1}$);
ρ density of the turbid layer ($M\ L^{-3}$);
ρ' density of the sand material ($M\ L^{-3}$);
ρ_0 density of the bed (mixture of sand and pore fluid) ($M\ L^{-3}$);
ρ_1 density of the turbid water influx ($M\ L^{-3}$);
ρ_∞ density of the receiving lake ambient ($M\ L^{-3}$);
$s(t)$ moving shoreline position (L);
S initial bed inclination;
$S_{\min}$ inclination threshold;
σ reduced horizontal coordinate;
σ' effective stress at the base of the bed load layer ($M\ L^{-1}\ T^{-2}$);
τ bottom shear stress ($M\ L^{-1}\ T^{-2}$);
u, v velocities of the turbid flow and bed load layer ($L\ T^{-1}$);
x horizontal coordinate (L);
ξ curvilinear distance measured along bed (L);
$z = z(x, t)$ evolving bed profile (L);
Z_0 prescribed bed elevation (L);
ζ lake level (L);
∂ partial differential.

[62] **Acknowledgments.** Financial support for this work was provided by the National Science Council and by the Tsung Cho Chang Educational Foundation, Taiwan. The experimental time-lapse photographs were acquired with the help of D. Douxchamps (Nara Institute of Science and Technology, Japan) and A. T. H. Perng (National Taiwan University). At National Taiwan University, F. C. Wu, D. L. Young, and L. S. Teng offered valuable feedback; Pei-Chen Hsu, Chun-Yao Hao, and Willy Wang contributed to exploratory experiments involving 1-D Gilbert deltas. Helpful comments and suggestions by J. B. Swenson are also gratefully acknowledged.

References

Adams, E. W., W. Schlager, and F. S. Anselmetti (2001), Morphology and curvature of delta slopes in Swiss lakes: Lessons for the interpretation of clinoforms in seismic data, *Sedimentology*, *48*, 661–679.

Begin, Z. B., D. F. Meyer, and S. A. Schumm (1981), Development of longitudinal profiles of alluvial channels in response to base level lowering, *Earth Surf. Processes Landforms*, *6*, 49–68.

Bell, H. S. (1942), Density currents as agents for transporting sediments, *J. Geol.*, *50*, 512–547.

Bellal, M., B. Spinewine, C. Savary, and Y. Zech (2003), Morphological evolution of steep-sloped river beds in the presence of a hydraulic jump: Experimental study, in *Proceedings of the XXX IAHR Congress*, vol. C-II, edited by J. Ganoulis and P. Prinos, pp. 133–140, Int. Assoc. of Hydraul. Eng. and Res., Madrid, Spain.

Bellal, M., C. Savary, and Y. Zech (2005), Morphological evolution of steep-sloped river beds in the presence of a hydraulic jump: Numerical and experimental analysis, in *Proceedings of the XXXI IAHR Congress*, edited by B. H. Jun et al., pp. 1522–1533, Int. Assoc. of Hydraul. Eng. and Res., Madrid, Spain.

Best, J. L., R. A. Kostaschuk, J. Peakall, P. V. Villard, and M. Franklin (2005), Whole flow field dynamics and velocity pulsing within natural sediment-laden underflows, *Geology*, *33*, 765–768.

Bornhold, B. D., and D. B. Prior (1990), Morphology and sedimentary processes on the subaqueous Noeick River delta, British Columbia, Canada, *Spec. Publ. Int. Assoc. Sedimentol.*, *10*, 169–181.

Capart, H., M. Bellal, L. Boxus, C. De Roover, and Y. Zech (1998), Approach to morphological equilibrium for steep-sloped river beds, in *Proceedings of the 7th International Symposium on River Sedimentation*, edited by A. W. Jayawardena, J. H. W. Lee, and Z. Y. Wang, pp. 231–237, A. A. Balkema, Rotterdam, Netherlands.

Capart, H., M. Bellal, and D. L. Young (2007), Self-similar evolution of semi-infinite alluvial channels with moving boundaries, *J. Sediment. Res.*, *77*, 13–22.

Carslaw, H. S., and J. C. Jaeger (1959), *Conduction of Heat in Solids*, Clarendon, Oxford, U. K.

Crank, J. (1984), *Free and Moving Boundary Problems*, Clarendon, Oxford, U. K.

Culling, W. E. H. (1960), Analytical theory of erosion, *J. Geol.*, *68*, 336–344.

Das, B. M. (1990), *Principles of Geotechnical Engineering*, PWS-KENT, Boston, Mass.

De Cesare, G., A. Schleiss, and F. Hermann (2001), Impact of turbidity currents on reservoir sedimentation, *J. Hydraul. Eng.*, *127*, 6–16.

Ellison, T. H., and J. S. Turner (1959), Turbulent entrainment in stratified flows, *J. Fluid Mech.*, *6*, 423–448.

Fan, J., and G. L. Morris (1992), Reservoir sedimentation I: Delta and density current deposits, *J. Hydraul. Eng.*, *118*, 354–369.

Fraccarollo, L., and H. Capart (2002), Riemann wave description of erosional dam-break flows, *J. Fluid Mech.*, *461*, 183–228.

García, M. H. (1993), Hydraulic jumps in sediment-driven bottom currents, *J. Hydraul. Eng.*, *119*, 1094–1117.

Gilbert, G. K. (1890), *Lake Bonneville*, *U.S. Geol. Surv. Monogr.*, *1*, 438 pp.

Graf, W. H. (1971), *Hydraulics of Sediment Transport*, McGraw-Hill, New York.

Grover, N. C., and C. S. Howard (1937), The passage of turbid water through Lake Mead, *Trans. ASCE*, *1994*, 720–732.

Hinderer, M. (2001), Late Quaternary denudation of the Alps, valley and lake fillings and modern river loads, *Geodin. Acta*, *14*, 231–263.

Hsu, S. T. (2006), Problems encountered in Shihmen reservoir and the improvement plans (in Chinese), paper presented at 1st Taiwan-Japan Workshop on Flood Hazard Mitigation, Kansai Electr. Power Co., Taipei, Taiwan.

Jordan, T. E., and P. B. Flemings (1991), Large-scale stratigraphic architecture, eustatic variation, and unsteady tectonism: A theoretical evaluation, *J. Geophys. Res.*, *96*, 6681–6699.

Kenyon, P. M., and D. L. Turcotte (1985), Morphology of a delta prograding by bulk sediment transport, *Geol. Soc. Am. Bull.*, *96*, 1457–1465.

Kim, W., C. Paola, V. R. Voller, and J. B. Swenson (2006), Experimental measurement of the relative importance of controls on shoreline migration, *J. Sediment. Res.*, *76*, 270–283.

Kleinhans, M. G. (2005), Autogenic cyclicity of foreset sorting in experimental Gilbert-type deltas, *Sediment. Geol.*, *181*, 215–224.

Kostic, S., and G. Parker (2003a), Progradational sand-mud deltas in lakes and reservoirs. part 1. Theory and numerical modeling, *J. Hydraul. Res.*, *41*, 127–140.

Kostic, S., and G. Parker (2003b), Progradational sand-mud deltas in lakes and reservoirs. part 2. Experiment and numerical simulation, *J. Hydraul. Res.*, *41*, 141–152.

Kostic, S., G. Parker, and J. G. Marr (2002), Role of turbidity currents in setting the foreset slope of clinoforms prograding into standing fresh water, *J. Sediment. Res.*, *72*, 353–362.

Kubo, Y., J. P. M. Syvitski, E. W. H. Hutton, and C. Paola (2005), Advance and application of the stratigraphic simulation model 2D-SedFlux: From tank experiment to geological scale simulation, *Sediment. Geol.*, *178*, 187–195.

Lai, S. Y. J. (2006), Self-similar delta formation by hyperpycnal flows: Theory and experiments, M. S. thesis, Grad. Inst. of Civ. Eng., Natl. Taiwan Univ., Taipei.

Lambert, A. (1982), Turbidity currents from the Rhine River on the bottom of Lake Constance (in German), *Wasserwirtschaft*, *72*, 1–4.

Lee, H.-Y., and W.-S. Yu (1997), Experimental study of reservoir turbidity current, *J. Hydraul. Eng.*, *123*, 520–528.

Lee, H.-Y., Y.-T. Lin, and Y.-J. Chiu (2006), Quantitative estimation of reservoir sedimentation from three typhoon events, *J. Hydraul. Eng.*, *11*, 362–370.

Marr, J. G., J. B. Swenson, C. Paola, and V. R. Voller (2000), A two-diffusion model of fluvial stratigraphy in closed depositional basins, *Basin Res.*, *12*, 381–398.

Mitchell, N. C. (2006), Morphologies of knickpoints in submarine canyons, *Geol. Soc. Am. Bull.*, *118*, 589–605.

Müller, G. (1966), The new Rhine delta in Lake Constance, in *Deltas in Their Geologic Framework*, edited by M. L. Shirley and J. E. Ragsdale, pp. 107–124, Houston Geol. Soc., Tex.

Müller, G., and U. Förstner (1966), General relationship between suspended sediment concentration and water discharge in the Alpenrhein and some other rivers, *Nature*, *217*, 244–245.

Muto, T. (2001), Shoreline autoretreat substantiated in flume experiments, *J. Sediment. Res.*, *71*, 246–254.

Muto, T., and J. B. Swenson (2005), Large-scale fluvial grade as a nonequilibrium state in linked depositional systems: Theory and experiment, *J. Geophys. Res.*, *110*, F03002, doi:10.1029/2005JF000284.

Paola, C. (2000), Quantitative models of sedimentary basin filling, *Sedimentology*, *47*, 121–178, suppl. 1.

Parker, G. (2004), *1D Sediment Transport Morphodynamics With Applications to Rivers and Turbidity Currents*, Natl. Cent. for Earth Surf. Dyn., Minneapolis, Minn.

Parker, G., and T. Muto (2003), 1D numerical model of delta response to rising sea level, in *Proceedings of the 3rd IAHR Symposium on River, Coastal and Estuarine Morphodynamics*, edited by A. Sanchez-Arcilla and A. Bateman, pp. 558–570, Taylor and Francis, London.

Posamentier, H. W., and G. P. Allen (1999), *Siliclastic Sequence Stratigraphy—Concepts and Applications, Concepts Sedimentol. Paleontol.*, vol. 7, 204 pp., Soc. for Sediment.Geol., Tulsa, Okla.

Roth, M., M. Weber, and G. R. Bezzola (2001), Physical modeling of sediment deposits in a river delta. Case study: The Alpenrhein Delta in Lake Constance, in *Proceedings of the XXIXth IAHR Congress*, edited by K. Yen and B. Lin, pp. 187–194, Int. Assoc. of Hydraul. Eng. and Res., Madrid, Spain.

Schumm, S. A. (1991), *To Interpret the Earth: Ten Ways to Be Wrong*, 133 pp., Cambridge Univ. Press, New York.

Smith, W. O., C. P. Vetter, and G. B. Cummings (1960), Comprehensive survey of sedimentation in Lake Mead, 1948–1949, *U.S. Geol. Surv. Prof. Pap.*, *295*, 253.

Swenson, J. B., V. R. Voller, C. Paola, G. Parker, and J. G. Marr (2000), Fluvio-deltaic sedimentation: A generalized Stefan problem, *Eur. J. Appl. Math.*, *11*, 433–452.

Syvitski, J. P. M., and J. M. Alcott (1993), GRAIN2: Predictions of particle size seaward of river mouths, *Comput. Geosci.*, *19*, 399–446.

Syvitski, J. P. M., and E. W. H. Hutton (2001), 2D SEDFLUX 1.0C: An advanced process-response numerical model for the fill of marine sedimentary basins, *Comput. Geosci.*, *27*, 731–753.

Syvitski, J. P. M. et al. (2007), Prediction of margin stratigraphy, in *Continental-Margin Sedimentation: Transport to Sequence*, edited by C. Nittrouer et al., Blackwell, Malden, Mass., in press.

Toniolo, H., and J. Schultz (2005), Experiments on sediment trap efficiency in reservoirs, *Lakes Reservoirs*, *10*, 13–24.

Turner, J. S. (1973), *Buoyancy Effects in Fluids*, Cambridge Univ. Press, New York.

Voller, V. R., J. B. Swenson, and C. Paola (2004), An analytical solution for a Stefan problem with variable latent heat, *Int. J. Heat Mass Transfer*, *47*, 5387–5390.

Wright, L. D., W. J. Wiseman, B. D. Bornhold, D. B. Prior, J. N. Suhayda, G. H. Keller, Z.-S. Yang, and Y. B. Fan (1988), Marine dispersal and deposition of Yellow River silts by gravity-driven underflows, *Nature*, *332*, 629–632.

Young, D. L., Q. H. Lin, and K. Murugesan (2005), Two-dimensional simulation of a thermally stratified reservoir with high sediment-laden inflow, *J. Hydraul. Res.*, *43*, 351–365.

Yu, W.-S., H.-Y. Lee, and S. M. Hsu (2000), Experimental study on delta formation in a reservoir (in Chinese), *J. Chin. Inst. Civ. Hydraul. Eng.*, *12*, 171–177.

H. Capart and S. Y. J. Lai, Dept. of Civil Engineering and Hydrotech Research Institute, National Taiwan University, Taipei 106, Taiwan. (hcapart@yahoo.com)